Researchers Journal of Science and Technology (REJOST)
https://rejost.com.ng

Predictive Hydrogeophysical Modelling of Subsurface Conditions Using Geo-Electrical Data Along a Water Channel in Akwa Ibom State, Southern Nigeria

Kufre R. Ekanem, Nyakno. J. George, Aniekan. M. Ekanem, Ndifreke I. Udosen, Jewel E. Thomas

Abstract

Groundwater exploration in alluvial and river-influenced terrains of Southern Nigeria is challenged by subsurface heterogeneity and the high cost of invasive drilling. This study presents a predictive hydrogeophysical modelling framework that integrates Vertical Electrical Sounding (VES), Electrical Resistivity Tomography (ERT), and machine learning to estimate deeper aquifer properties from shallow resistivity data along the Kwa Iboe River channel. A total of 27 VES and 9 ERT profiles were analyzed to characterize geo-electrical parameters. Machine learning models, including Random Forest, Neural Networks, and Ridge Regression, were evaluated for predicting deeper resistivity, porosity, hydraulic conductivity, transmissivity, and aquifer thickness. Random Forest achieved superior accuracy (R^2 = 0.92–0.96) in resistivity prediction, while Ridge Regression performed best for aquifer thickness (R^2 = 0.75). The results delineated high-yield zones with low resistivity (<20 Ωm) and high transmissivity (>1000 m²/day), mainly near the river. Strong correlations were observed between resistivity and hydrokinetic parameters (e.g., r = 0.99 between ρ_b and ρ_w). Spatial maps illustrated aquifer behavior influenced by lithology, topography, and river recharge. This integrated, data-driven approach offers a cost-effective alternative to traditional drilling, aiding sustainable groundwater development and environmental planning in tropical, riverine settings.

✉ Kufre R. Ekanem: ekanemkufre03@gmail.com
Department of Physics (Geophysics Research Group), Akwa Ibom State University, Mkpat Enin, Uyo, PMB 1162, Nigeria

Keywords: Geo-resistivity, predictive modelling, machine learning, Random Forest, Neural network am linear regressor

Article history
Received: April 26, 2025
Received in revised form: July 23, 2025
Accepted for publication: August 2, 2025
Available online: August 5, 2025

1.0 Introduction

Predictive hydrogeophysical modelling has become an essential tool for understanding subsurface conditions in areas with complex hydrogeology and limited baseline data (Driba *et al*., 2024). By integrating geophysical observations with hydrological interpretations, it enables spatially explicit forecasting of subsurface parameters critical for groundwater development and environmental planning. The combined application of Vertical Electrical Sounding (VES) and Electrical Resistivity Tomography (ERT) offers a robust approach to subsurface investigation (Ibuot *et al*., 2017). While VES provides deep penetration for vertical profiling, ERT delivers high-resolution imaging of lateral variations. Together, they offer a comprehensive view of lithological structures and groundwater pathways, particularly useful in heterogeneous and dynamic terrains. Water channels, including streams, rivers, and seasonal drainages, significantly influence hydrostratigraphy through infiltration and recharge processes. In tropical, flood-prone regions, like parts of Southern Nigeria, interactions between surface water and subsurface materials often lead to environmental challenges including erosion, flooding, and borehole failures. Understanding these interactions is essential for effective land-use planning and groundwater resource management (Adelana & Taylor, 2008).

Akwa Ibom State, located within the coastal sedimentary basin of the Niger Delta, is characterized by alluvial deposits, variable lithologies, and complex geomorphology. Although groundwater is heavily relied upon for domestic and agricultural use, especially in rural and peri-urban areas, predictive knowledge of the subsurface remains limited-particularly along its numerous riverine environments. This lack of detailed hydrogeophysical data often results in unsuccessful borehole siting and poor resource management (George et al., 2021b).

This study aims to address this knowledge gap by developing a predictive hydrogeophysical model along a selected water channel in Akwa Ibom State using integrated VES and ERT datasets. The specific objectives are to: (1) conduct detailed geophysical surveys, (2) delineate subsurface lithological and structural features, (3) analyze geo-electric parameters to identify aquifer units and groundwater pathways, (4) construct a predictive model for aquifer potential and subsurface zoning, and (5) assess the implications of the findings for groundwater development and environmental management. By providing high-resolution subsurface imaging and predictive insights, this research will support informed water resource planning, mitigate borehole failure risks, and contribute to sustainable environmental practices in one of Nigeria's hydrogeologically vulnerable regions (Ibuot *et al*., 2024).

2.0 Study Area Description

This study was carried out along a selected water channel in southern Akwa Ibom State, Nigeria, a region situated within the Niger Delta sedimentary basin as opined by Emmanuel (2013) in Fig. 1. Geographically, the area extends approximately between latitudes 4°33′N and 5°33′N and longitudes 7°35′E and 8°25′E. The specific segment investigated lies within a hydrologically active corridor where surface water-aquifer interactions are prominent. This corridor, characterized by low-lying terrain and moderate-to-high recharge potential, is located within the Gulf of Guinea.

The geology of the study area is dominated by Coastal Plain sands or the Benin Formation (Miocene to Recent), part of the upper Niger Delta sequence (Fig. 1). This formation consists primarily of unconsolidated coarse- to medium-grained sands, interbedded with clay and silt layers, indicative of fluvial and deltaic depositional environments (Ikpe *et al*., 2025). These sediments form highly permeable aquifers with considerable groundwater storage capacity.

However, the intercalation of clay units introduces heterogeneity, which can inhibit lateral groundwater flow and complicate aquifer connectivity (George *et al*., 2024).

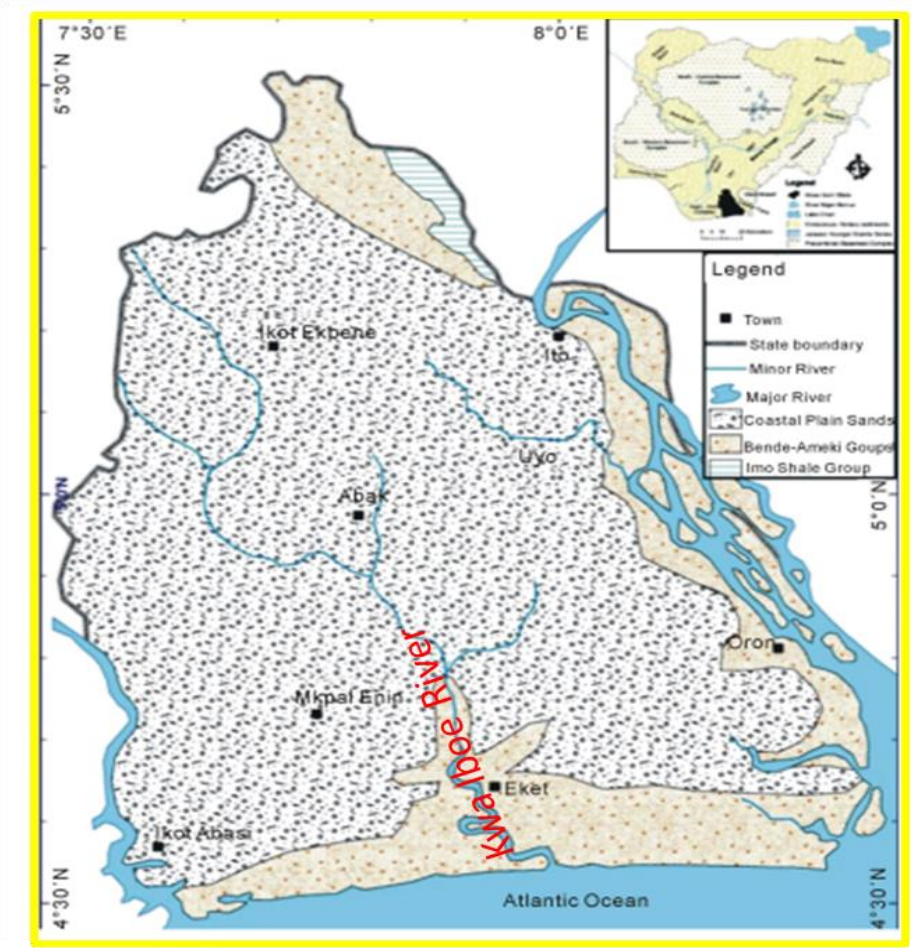

Fig. 1: Map of the study area, Akwa Ibom State, Nigeria showing the Kwa Iboe River and the geology of the study area (Adapted from Emmanuel, 2013).

Climatically, the region experiences a tropical humid climate, marked by a prolonged wet season (March to October) and a short dry season (November to February). Annual rainfall ranges from 2,000 mm to 3,500 mm, with temperatures typically between 26°C and 32°C (Ekanem *et al*., 2022a). This climate fosters substantial groundwater recharge, surface runoff, and extensive drainage development. Seasonal variations in precipitation significantly affect water table levels and subsurface moisture content. The drainage system follows a dendritic to sub-parallel pattern, controlled by both topography and subsurface lithology. Numerous first- to third-order streams converge into larger tributaries that eventually discharge into the Atlantic Ocean. These channels are instrumental in recharging shallow aquifers and modulating surface-subsurface hydrological dynamics, especially during peak rainfall periods. Soil types within the study area are predominantly ferrallitic and hydromorphic, derived from the weathering of sandstone and clayey parent materials. Ferrallitic soils are well-drained, reddish-brown, and sandy, supporting effective infiltration, while hydromorphic soils are poorly drained, clayey, and greyish, often associated with seasonal waterlogging and reduced structural stability for construction and agriculture (Onwumechili, & Okonkwo, 2013). The choice of this water channel was informed by two primary factors: hydrological significance and logistical feasibility. The channel serves as a key tributary in the regional

watershed, displaying evident hydraulic connectivity with surrounding shallow aquifers, making it ideal for geophysical investigation. Its position within a transitional physiographic zone heightens its relevance for studying recharge and discharge processes. Additionally, the site offers year-round accessibility, and cut across the study area investigated.

Given the complex hydrogeological context, the application of integrated Vertical Electrical Sounding (VES) and Electrical Resistivity Tomography (ERT) techniques in this setting enables high-resolution characterization of the subsurface (Inim *et al.*, 2020). This integrated geophysical approach supports the prediction of aquifer geometry, identification of lithological heterogeneities, and mapping of groundwater flow pathways and structural features, all essential for guiding sustainable groundwater development in vulnerable coastal environments (Ekanem *et al*., 2022b).

3.0 Material and method

3.1 Field Methods

This georesistivity-based study investigates the lithological and hydrodynamic parameters influencing groundwater sanitation across aquifer systems situated along the Akwa Ibom river channels and their tributaries. The methodology integrates 27 Vertical Electrical Soundings (VES) and 9 Electrical Resistivity Tomography (ERT) profiles to evaluate the subsurface conditions affecting groundwater quality and movement near these fluvial networks. The selection of VES locations was guided by hydrogeological indicators, such as the spatial distribution of existing boreholes, proximity to surface water channels, and physical inaccessibility of certain terrain units. These soundings were spatially distributed to provide thorough coverage of aquifer-prone zones, especially areas influenced by surface-subsurface interactions. For subsurface probing, the Schlumberger array configuration was adopted (Anomohanran, 2011). Measurements began with a minimum current electrode separation (AB/2) of 0.5 meter and extended progressively up to 200 meters. This expansion in electrode spacing enabled deeper geoelectrical penetration and more accurate delineation of aquifer boundaries, lithological transitions, and zones potentially susceptible to contamination (George *et al*., 2025). At each VES station, apparent resistance (R_a) was recorded using a resistivity meter (Fig. 2). The corresponding Schlumberger apparent resistivity (ρ_{as}) was calculated using standard formulas dependent on the electrode geometry, particularly the relationship between inner (MN/2) and outer (AB/2) electrode spacing, as expressed in Equations 1 to 3:

$$R_a = \frac{\Delta V}{I} \quad (1)$$

$$\rho_{as} = \pi \times \left(\frac{\left(AB/2\right)^2 - \left(MN/2\right)^2}{MN} \right) \times \frac{\Delta V}{I} \quad (2)$$

$$\rho_{as} = G_s \times R_a \quad (3)$$

In this context, *Gs* denotes the geometric factor, determined by electrode spacing, and used to calculate apparent resistivity values. When *AB/2 = a* and *MN/2 = b*, the geometric factor (G_s) for the Schlumberger configuration is expressed by the right-hand terms in equation 2 that multiplies R_a *or* $\frac{\Delta V}{I}$. In terms of a and *b*, the apparent resistivity for Schlumberger configuration can also be expressed using equation 2 as shown in equation 4:

$$\rho_{as} = \pi \left(\frac{a^2}{b} - \frac{b}{4} \right) \frac{\Delta V}{I} \quad (4)$$

where geometric factor $G_s = \pi \left(\frac{a^2}{b} - \frac{b}{4} \right)$. For 2D ERT measurements, the Wenner array configuration was also utilized, with the geometric factor ($G_w = 2\pi a$).

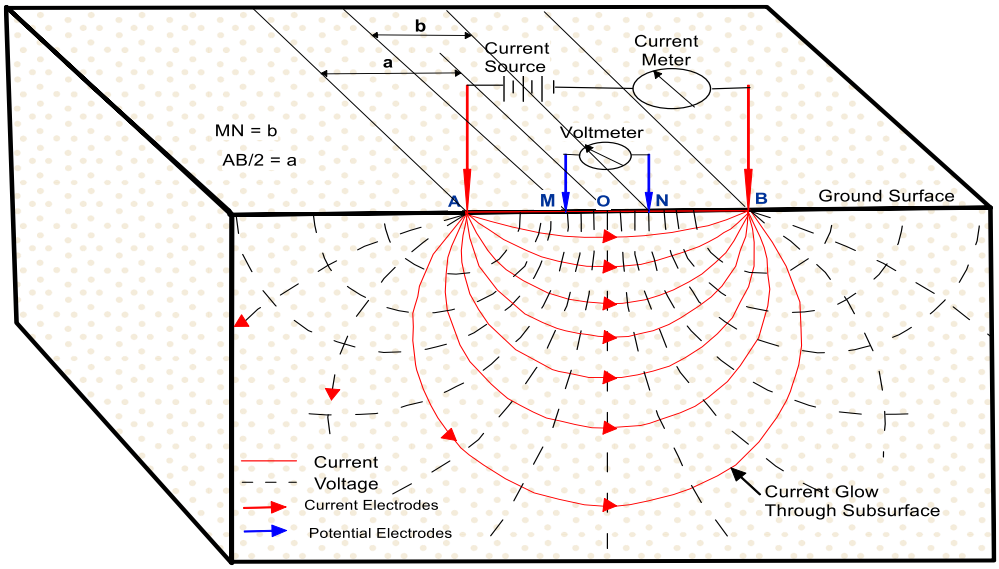

Fig. 2: Diagram schematically illustrating the arrangement in geo-electrical resistivity operation

The apparent resistivity for the uniform electrode spacing was calculated using apparent Wenner resistance R_w equation 5:

$$\rho_{as} = G_s \times R_a \quad (5)$$

These geometric factors allowed for accurate computation of resistivity values in varying configurations, tailored to different survey depths and resolution requirements (see Fig. 2) for electrode arrangement.

3.2 Data Acquisition and Processing Workflow

The VES technique was adopted owing to its proven effectiveness in characterizing vertical and lateral variations in subsurface resistivity, which is critical in identifying economically viable aquifer zones (George *et al*., 2016; George *et al*., 2021a; Asfahani *et al.*, 2023). A resistivity meter configured for both the Schlumberger and Wenner arrays was used to acquire the field data. To validate the geophysical interpretations, ground-truth data including borehole logs and hydrogeological records were incorporated (Udosen *et al*., 2024 a, b, c). Apparent resistivity values derived from the Schlumberger array (for VES) and Wenner array (for ERT) were computed using Equations 4 and 5, respectively. Prior to interpretation, the raw datasets were subjected to data smoothing and noise filtering to eliminate spurious anomalies not consistent with expected geological formations. Subsequently, the processed data were analyzed using the WINRESIST software for 1D VES interpretation and RES2DINV for 2D ERT inversion. These software tools implement iterative least-squares inversion algorithms to fit model responses to observed field data. Up to 28 iterations were executed to achieve optimal model convergence (George *et al*., 2022a). A Root Mean Square Error (RMSE) threshold of ≤10% was maintained throughout the modeling process to ensure high confidence in the derived subsurface models (George *et al*., 2022b; Asfahani et al., 2023). The 1D VES interpretations yielded parameters such as true resistivity, layer thickness, and depth to interfaces, which were validated against borehole data (Fig. 3) (Ibanga & George, 2016). Complementary 2D ERT profiles, particularly with electrode spreads up to 105 m AB, provided enhanced resolution and subsurface imaging, facilitating better delineation of aquifer geometries and variations in moisture content and lithology (Ghouili *et al*., 2020).

By integrating these datasets, the study was able to delineate the geoelectric primary indices (resistivity, thickness, and depth) (Table 1), identify zones of enhanced aquifer potential, detect variations in lithological composition, and

understand the influence of shallow subsoil and relatively deep subsoil and their subsurface hydrodynamics (Inyang *et al.*, 2024). This integrative approach offered a robust hydrogeophysical framework for evaluating geo-resistivity predictive modelling, and guiding the systemic influence of pre-aquifer and aquifer layer for groundwater management in the region (Freeze & Cherry, 1979; Udosen *et al.*, 2024a).

3.3 Hydrokinetic Parameters

Hydrodynamic evaluation for groundwater sanitation begins with data from Vertical Electrical Soundings (VES), complemented by pore water resistivity and formation-specific constants (Uwa *et al.*, 2019). These inputs facilitate the estimation of key subsurface flow properties - porosity, permeability, and hydraulic conductivity, which are critical in understanding aquifer response near water channels. These parameters offer insight into groundwater movement and natural filtration processes vital for water quality (George *et al.*, 2015b). Their interrelationship, governed by Archie's law (1942) and shown in Equation 6, links bulk resistivity, water resistivity, effective porosity, cementation, and tortuosity factors. This method enhances the prediction of contaminant pathways and supports effective groundwater sanitation planning (Ekanem *et al.*, 2025; George *et al.*, 2025).

$$\phi = \left(\frac{a}{F}\right)^{\frac{1}{m}} \qquad 6$$

For unconsolidated sandy aquifers with an average grain size of 0.00061 m (range: 0.00035–0.00097 m, measured via digital micrometer), key physical constants include a water density of 1000 kg/m³, dynamic viscosity of 0.0014 kg·m^{-1}·s^{-1} (Fetters, 1994), and gravitational acceleration of 9.81 m/s². Formation water resistivity (ρ_w) was computed using Umoh *et al.*'s (2022) empirical model, where $\rho_w = 0.05777\rho + 13.643$ for $\rho > 13.643$, and $\rho_w = 0.05777\rho$ for lower values, derived under similar geologic conditions in the study area.

The formation factor ($F = \rho_b/\rho_w$), in conjunction with porosity (ϕ), informs tortuosity (τ), calculated as $\tau = \sqrt{(F\phi)}$. Constants a = 0.5245 and m = 1.5431 from George *et al.* (2015a) reinforced the positive link between porosity and hydraulic conductivity (K), aligning with the Kozeny–Carman model (Kozeny, 1927; Carman, 1937, 1956) as presented in Equations 7–9. These interdependent parameters, grain size, resistivity, porosity, and permeability, form the backbone of predictive hydrogeophysical modelling. They offer vital insights into subsurface important parameters used in flow characteristics. The relationship with porosity enabled the estimation of aquifer system hydrokinetic variables identified in Equations 7-10:

$$K = \left(\frac{\delta_w g}{\mu_{dv}}\right)\left(\frac{\phi^3}{(1-\phi)^2}\right)\left(\frac{d_m^2}{180}\right) = \left(\frac{\delta_w g}{\mu_{dv}}\right)\left(\frac{d^2}{180}\right)\left(\phi\phi_N^2\right) \qquad (7)$$

$$K_p = \frac{d_m^2\phi^3}{180(1-\phi)^2} = \left(\frac{d_m^2}{180}\right)\left(\phi_N^2\phi\right) \qquad (8)$$

where ϕ_N is the normalized porosity given by

$$\phi_N = \frac{\phi}{1-\phi} \qquad (9)$$

and K_p is the permeability. Hydraulic conductivity (Kp), initially expressed in m², was converted to millidarcies (mD) using the factor 1.01325×10^{15} mD/m² for better relevance to water sanitation studies. To assess aquifer index of performance, transmissivity (T) was calculated by multiplying aquifer thickness (h) with hydraulic conductivity (Kh), following the approach in Equation 10.

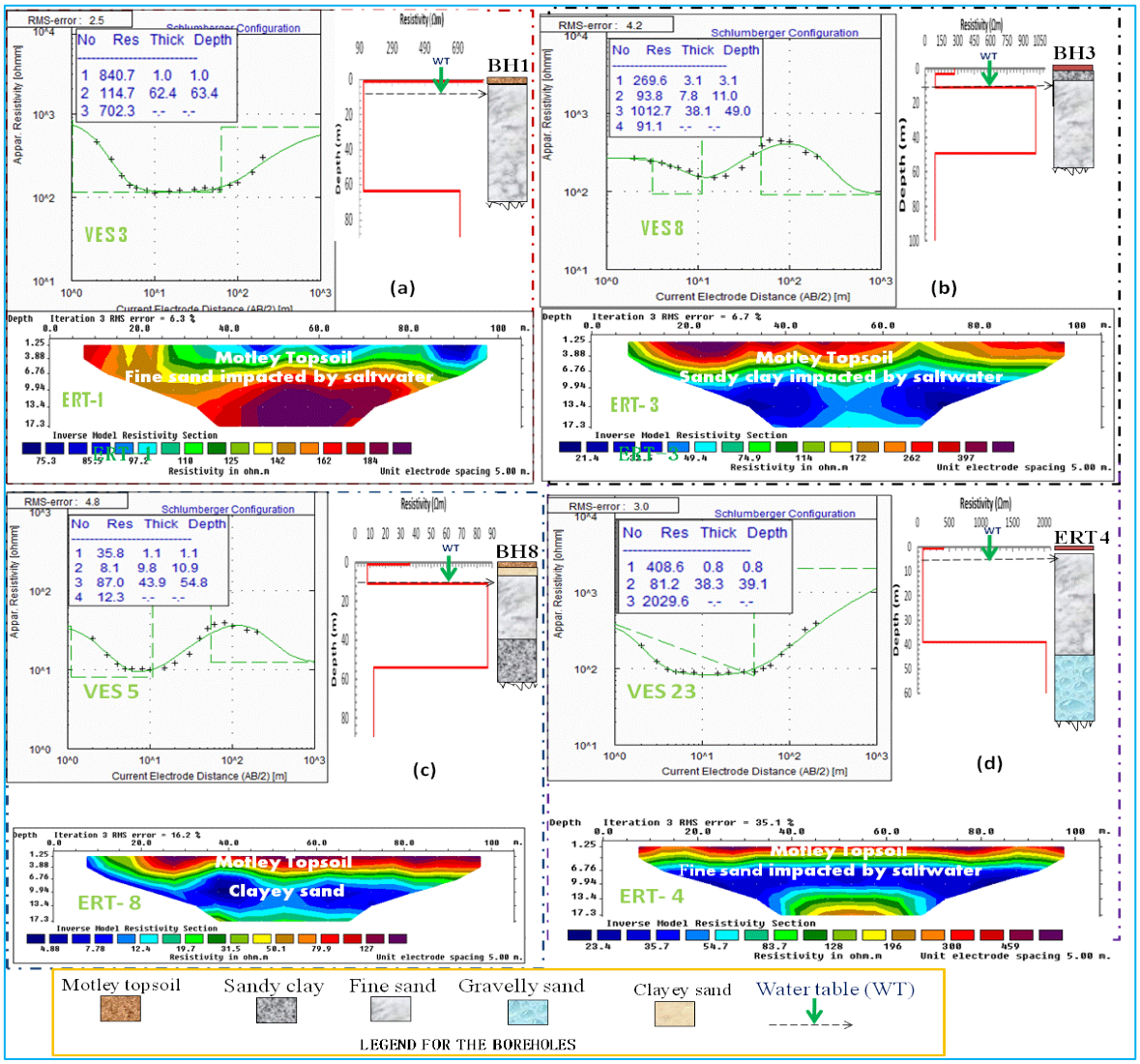

Figure 3: Correlations of selected interpreted VES curves, ERT sections, and nearby lithology logs near (a) Oron Museum: VES 3, ERT 1, and Borehole 1; (b) Esit Eket pipeline: VES 8, ERT 3, and Borehole 3; (c) Okoroete-Eastern Obolo: VES 5, ERT 8, and Borehole 8; and (d) Ibawa Abak 1: VES 23, ERT 4, and Borehole 4, within the investigated river channel

This provides a clearer understanding of aquifer system capacity and its implications for water quality and resource management (Etu-Efeotor & Akpokodje, 1990).

$$T = K_h h \quad (10)$$

Table 2 summarizes the estimated hydrokinetic parameters, while Table 3 presents the transmissivity classification based on groundwater yield potential (George, 2020). This classification is key to understanding aquifer performance and water movement, critical factors in evaluating groundwater suitability for sustainable and sanitary water supply near water channel (George *et al.*, 2016). The geo-resistivity and hydrodynamic parameters were used to create potential maps, which shows the spatial spread of parameters with the pre- aquifer and aquifer system in the study area (Figs. 5-7). This study adopts an integrated hydrogeophysical predictive modelling approach aimed at estimating key aquifer properties across subsurface formations adjacent to water channels in Akwa Ibom State, Southern Nigeria (see Fig. 4). The methodology combines field-based geoelectrical data acquisition with advanced machine learning algorithms to enable non-invasive, data-driven assessment of hydrogeological characteristics critical for groundwater exploration and management.

Table 1: Summary of Geo-resistivity data

VES /ERT No	VES location	BH No	Long. (deg.)	Lat. (deg.)	Elev. (m)	Resistivity (Ωm)				Thickness (m)			Depth (m)		
						ρ_1	ρ_2	ρ_3	ρ_4	h_1	h_2	h_3	d_1	d_2	d_3
1	Uya Oron 1		8.3446	4.8158	21	284.1	80.7	412.8	860.1	0.6	8.1	63.8	0.6	8.7	72.5
2	Uya Oron 2		8.2778	4.855	17	52.7	270	91.2	-	4.4	87.2	-	4.4	91.6	-
3/1	Oron Museum 3	1	8.3049	4.9117	17	840.7	114.7	702.3	-	1	62.4		1	63.4	
4	Oron 4		8.3028	4.8595	5	14.1	8.3	1.1	-	2.5	53.6		2.5	56.2	
5/8	Okoroete Eastern Obolo	8	7.888	4.6499	5	35.8	8.1	87	12.3	1.1	9.8	43.9	1.1	10.9	54.8
6	Mpat Enin		7.8851	4.771	4	896.6	303	61.3	-	14.1	47.1		14.1	61.2	
7	Unna		8.0047	4.6538	7	545	68.5	415.4	72.1	2.6	20.6	56.9	2.5	23.2	80.1
8/3	EsitEket pipeline	3	8.1294	4.7384	7	269.6	93.8	1012.7	91.1	3.1	7.8	38.1	3.1	11	49
9	Eket1		8.0773	4.7906	14	357.8	140	911.1	150.2	4.5	8.3	37.5	4.5	12.8	50.2
10	Eket 2		8.0334	4.7739	2	117.4	956	1971.6	-	1.5	102.8	-	1.5	104.3	-
11	Eket 3		8.0146	4.7948	4	147.9	20.5	84.6	-	2.7	91.7	-	2.7	94.4	-
12	Uta Ewa Ikot Abasi 1	7	7.7056	4.6788	7	163.4	19.5	2408.9	209.3	0.9	1.8	36	0.9	2.7	38.7
13/7	Uta Ewa Ikot Abasi 2		7.7145	4.7248	1	36	12.4	7.3		4.2	89.2	-	4.2	93.4	-
14	Ukpum Ete, Ikot Abasi 3		7.7799	4.6344	2	304.8	19.2	7.7	28.1	1.3	7	46.3	1.3	8.3	54.6
15	Ikot Abasi 4		7.7306	4.6235	6	995.9	93	495	66.2	2.3	8.5	26	2.3	10.8	36.8
16/2	EnwangEnwang 1	2	8.3343	4.7447	8	222.2	13.4	51	-	1.4	34	-	1.4	35.4	-
17	Mbo 2		8.2631	4.753	12	510.2	116.8	12.6	88.4	1	13.1	56.4	1	14.1	70.5
18/10	Ibeno Beach	10	8.2519	4.6619	30	972.5	1847.1	540	-	5	71.9	-	5	76.9	-
19	Upenekang, Ibeno		8.0506	4.6695	31	2345.4	886.1	120.8	-	1.5	56.6	-	1.5	58.1	-
20/6	Uyo village Rd 1	5, 6	8.0164	5.1623	15	152.2	19.1	238	71.3	0.9	15.3	74.5	0.9	16.2	90.7
21	Ntak Inyang, Itu		8.0647	5.1874	14	922	266.9	1129.1	623.4	0.6	15.5	79.7	0.6	16	95.7
22/5	Nwaniba Uyo 2		7.9833	5.1247	4	1110.1	165.2	584.7	2128.2	0.6	4.3	54.4	0.6	4.9	59.3
23/4	Ibawa, Abak 1	4	7.9164	5.1185	12	408.6	81.2	2029.6	-	0.8	38.3	-	0.8	39.1	-
24	Ibawa, Abak 2		7.8496	5.0905	27	452.2	75.4	190.3	24	8.2	19.1	39.5	8.2	27.3	66.8
25	Ediene Abak		7.7995	5.1011	23	1196.5	241.4	2178.3	2025.4	3.3	12.2	53.4	3.3	15.5	68.9
26/9	Ifianyong, Beach Uruan LGA 1		8.1441	5.1373	4	121.5	17.8	235.5	45.9	1.1	15.3	66.5	1.1	16.4	82.9
27	Ifianyong UsukUruan LGA 2		8.165	5.0746	12	55	115.5	36.5	999.8	1.4	14.9	26.3	1.4	16.2	42.5
Range					1-31	14.1-2345.4	8.1-1847.1	1.1-2408.9	12.3-2128.2	0.6-14.1	1.8-102.8	26.0-97.7	0.6-14.1	2.7-104.3	36.8-95.7
Mean					11.5	501.1	224.2	593.2	468.5	2.9	33.9	50	2.9	36.6	63.4
SD					8.7	524.2	400.9	736.2	699.9	2.7	31.6	16	2.9	32.3	18.1
CV (SD/ Average) %					78	105	179	124	149	93	93	32	107	88	29

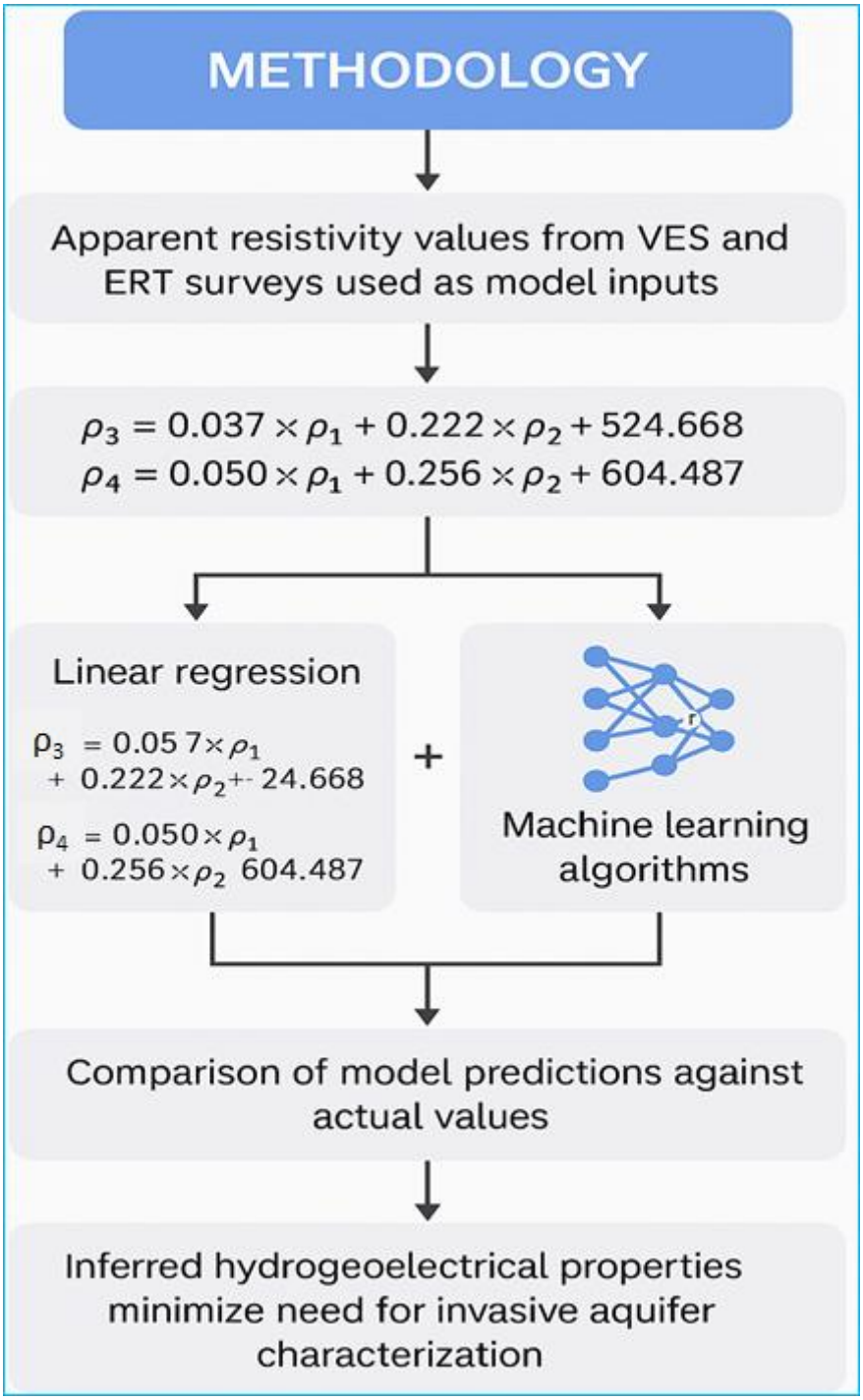

Fig. 4: Flowchart showing the methodology used in predictive modelling of geo-resistivity system within the Akwa Ibom State water channel

Table 2: Computed Summary of probable and economic aquifer system hydrodynamic properties at various VES stations surveyed and groundwater supply and designation according to Okogbue, and Omonona (2013)

VES	ρ_b (Ω m)	h (m)	d (m)	ρ_w (Ω m)	F	F	τ	K (m/day)	K (m/s)	K_p (mD)	T (m^2/day)	Designation based on Transmissivity	Groundwater Supply Potential
1	412.8	63.8	72.5	37.49	0.139	11	1.2	1.73	0.00002	2847.38	110.37	High	Withdrawal of lesser regional importance
2	270	87.2	91.6	29.24	0.156	9.2	1.2	2.33	2.7E-05	3878.57	203.18	High	Withdrawal of lesser regional importance
3	114.7	62.4	63.4	20.27	0.214	5.7	1.1	4.41	5.1E-05	7233.39	275.18	High	Withdrawal of lesser regional importance
4	8.3	53.6	56.2	0.48	0.104	17.3	1.3	29.81	0.00035	48934.5	1597.82	Very High	Withdrawal of great regional importance
5	87	43.9	54.8	18.67	0.243	4.7	1.1	5.36	6.2E-05	8845.74	235.3	High	Withdrawal of lesser regional importance
6	303	47.1	61.2	31.15	0.151	9.7	1.2	2.16	2.5E-05	3566.27	101.74	High	Withdrawal of lesser regional importance
7	415.4	56.9	80.1	37.64	0.139	11	1.2	1.73	0.00002	2834.4	98.44	Intermediate	Withdrawal of local water supply (Small community, plant etc.)
8	1012.7	38.1	49	72.15	0.119	14	1.3	0.86	0.00001	1481.54	32.77	Intermediate	Withdrawal of local water supply (Small community, plant etc.)
9	911.1	37.5	50.2	66.28	0.12	13.7	1.3	0.95	1.1E-05	1600.07	35.63	Intermediate	Withdrawal of local water supply (Small community, plant etc.)
10	956	102.8	104.3	68.87	0.12	13.9	1.3	0.95	1.1E-05	1545.01	97.66	Intermediate	Withdrawal of local water supply (Small community, plant etc.)
11	20.5	91.7	94.4	14.83	0.534	1.4	0.9	15.47	0.00018	25336.6	1418.6	Very High	Withdrawal of great regional importance
12	2408.9	36	38.7	152.8	0.11	15.8	1.3	0.52	6E-06	788.39	18.72	Intermediate	Withdrawal of local water supply (Small community, plant etc.)
13	12.4	89.2	93.4	0.72	0.104	17.2	1.3	22.29	0.00026	36533.7	1988.27	Very High	Withdrawal of great regional importance
14	7.7	46.3	54.6	0.44	0.104	17.5	1.3	31.45	0.00036	51682	1456.14	Very High	Withdrawal of great regional importance
15	495	26	36.8	42.24	0.134	11.7	1.3	1.56	1.8E-05	2494.78	40.56	Intermediate	Withdrawal of local water supply (Small community, plant etc.)
16	13.4	34	35.4	0.77	0.104	17.4	1.3	21	0.00024	34528.1	714	High	Withdrawal of lesser regional importance
17	12.6	56.4	70.5	0.73	0.104	17.3	1.3	22.03	0.00026	36110.6	1242.49	Very High	Withdrawal of great regional importance
18	1847.1	71.9	76.9	120.4	0.112	15.3	1.3	0.6	7E-06	956.53	43.14	Intermediate	Withdrawal of local water supply (Small community, plant etc.)
19	886.1	56.6	58.1	64.83	0.121	13.7	1.3	1.04	1.2E-05	1632.81	58.86	Intermediate	Withdrawal of local water supply (Small community, plant etc.)
20	238	74.5	90.7	27.39	0.162	8.7	1.2	2.59	0.00003	4251.64	192.96	High	Withdrawal of lesser regional importance
21	1129.1	79.7	95.7	78.87	0.117	14.3	1.3	0.86	0.00001	1368.72	68.54	Intermediate	Withdrawal of local water supply (Small community, plant etc.)
22	584.7	54.4	59.3	47.42	0.129	12.3	1.3	1.38	1.6E-05	2209.92	75.07	Intermediate	Withdrawal of local water supply (Small community, plant etc.)
23	81.2	71.9	39.1	18.33	0.251	4.4	1.1	5.7	6.6E-05	9301.38	409.83	High	Withdrawal of lesser regional importance
24	190.3	39.5	66.8	24.64	0.175	7.7	1.2	3.02	3.5E-05	5003.49	119.29	High	Withdrawal of lesser regional importance
25	2178.3	53.4	68.9	139.5	0.111	15.6	1.3	0.52	6E-06	848.31	27.77	Intermediate	Withdrawal of local water supply (Small community, plant etc.)
26	235.5	66.5	82.9	27.25	0.163	8.6	1.2	2.59	0.00003	4284.45	172.24	High	Withdrawal of lesser regional importance
27	36.5	26.3	42.5	15.75	0.382	2.3	0.9	10.11	0.00012	16647.7	265.89	High	Withdrawal of lesser regional importance
Range	7.7-2408.9	26.0-102.6	35.4-104.3	0.44-152.81	0.104-0.54	1.4-17.5	0.9-1.3	0.52-31.45	0.000006-0.00036	788.39-51682	18.72-1988.27		
Mean	550.7	58.1	66.2	42.9	0.164	11.5	1.2	7.2	8.3E-05	11731.3	411.1		
SD	675.8	20.6	20.3	41.4	0.096	4.8	0.1	9.6	0.00011	15747.1	577.9		
CV (%)	123	36	37	97	59	42	10	133	134	134	141		

Table 3: The classification of transmissivity based on supply potential (after Krasny, 1993)

Transmissivity my^2/day	Designation	Designation Groundwater Supply Potential
>1000	Very hgh	Withdrawal of great regional importance
100-1000	High	Withdrawal of lesser regional importance
10-100	Intermediate	Withdrawal of local water supply (Small community, plant etc.)
1-10	Low	Smaller withdrawal for local water supply (Private consumption)
0.1-1	Very low	Withdrawal for local water supply (Private consumption)
<0.1	Impermeable	Sources for local water supply are difficult

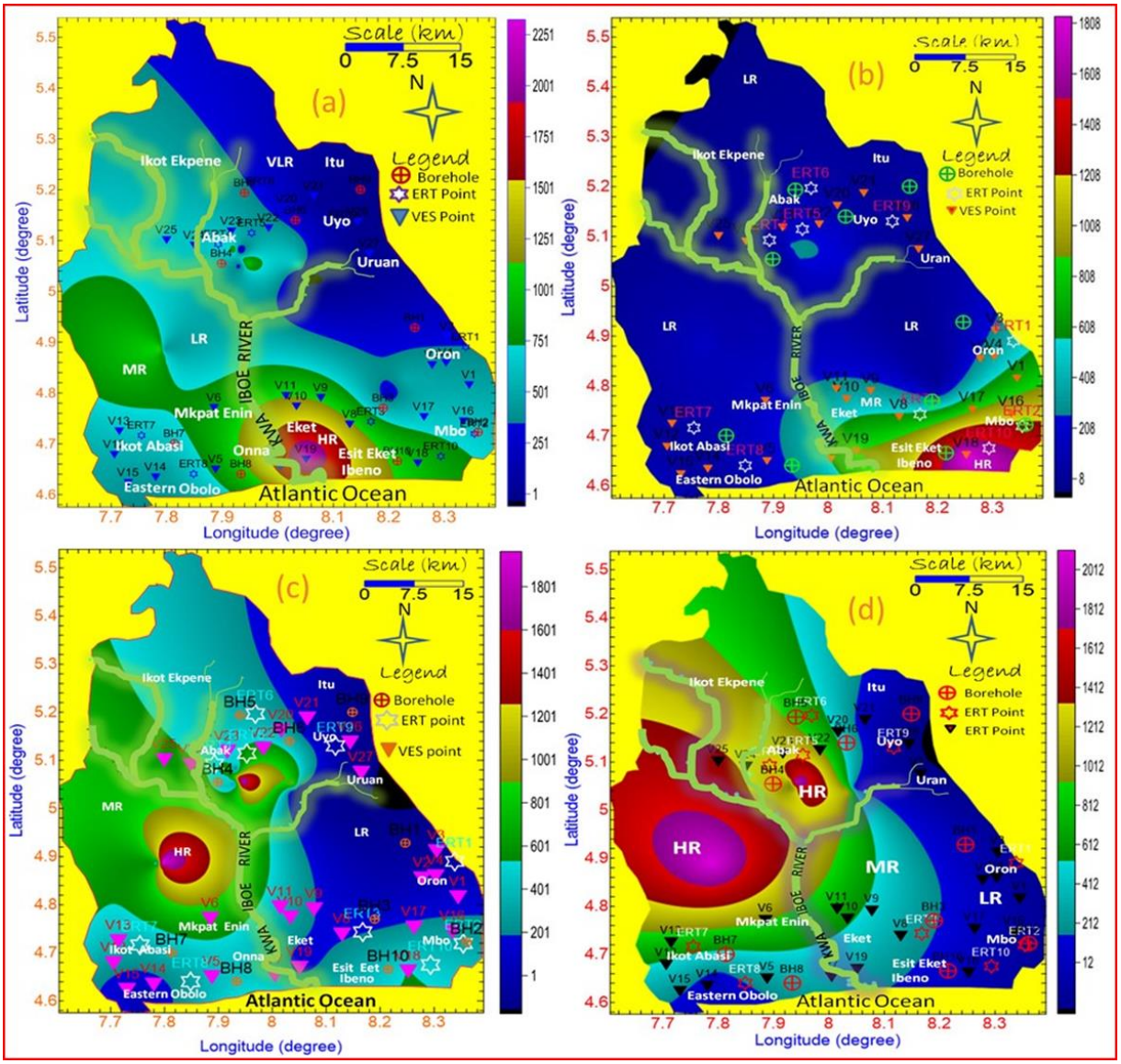

Fig. 5: Diagram illustrating the geo-resistivity distributions in (a) layer 1, (b) layer 2, (c) layer 3, and (d) layer 4, as influenced by currents within the freshwater Kwa Iboe River channels (KIRC). The areas are marked by low resistivity (LR), moderate resistivity (MR), and high resistivity (HR).

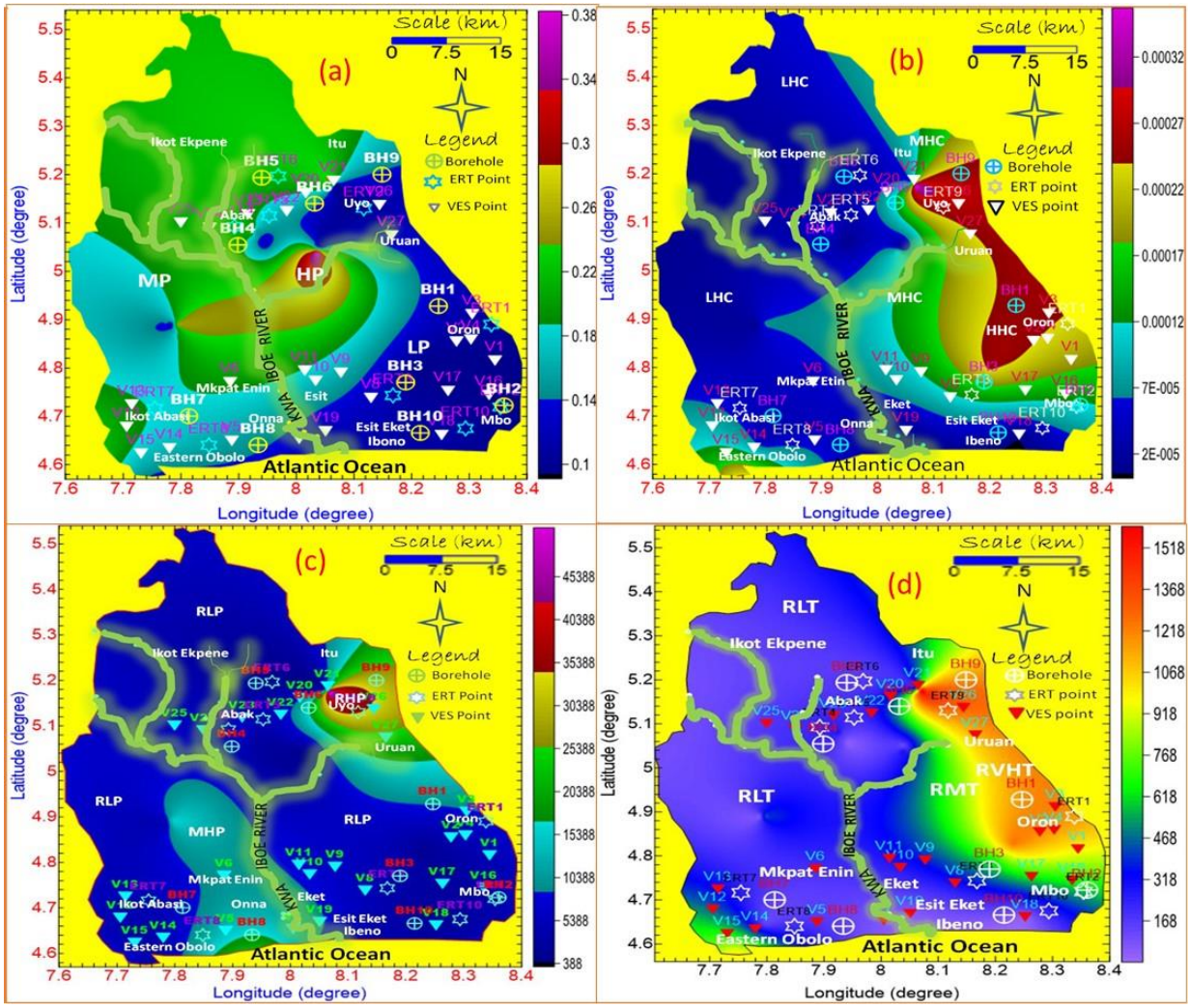

Fig. 6: Diagram illustrating the hydrodynamic properties of aquifer systems in the Kwa Iboe water channels: (a) Aquifer porosity, (b) Hydraulic conductivity, (c) Permeability, and (d) Transmissivity. The river channel aquifers are categorized by low porosity (LP), moderate porosity (MP), and high porosity (HP), as well as by hydraulic conductivity (low hydraulic conductivity [LHC], moderate hydraulic conductivity [MHC]), permeability (relatively low permeability [RLP], moderately high permeability [MHP]), and transmissivity (relatively low transmissivity [RLT], moderate transmissivity [RMT], and relatively very high transmissivity [RVHT]).

3.4 Predictive modelling

The modelling process commenced with the utilization of geoelectrical resistivity data, complemented by secondary parameters derived from primary geoelectrical indices. Vertical Electrical Sounding (VES) provided high-resolution vertical profiling of resistivity variations, while Electrical Resistivity Tomography (ERT) offered detailed lateral imaging of subsurface structures. Together, these techniques captured the electrical signatures associated with lithological heterogeneity, moisture content, and fluid conductivity, thereby establishing a robust foundation for interpreting the geoelectrical framework of the study area. The resulting resistivity values, denoted as ρ_1, ρ_2, ρ_3, and ρ_4, served as key input variables for the development of the predictive model.

Subsequently, mathematical regression models and supervised machine learning techniques, particularly Random Forest Regressors and Artificial Neural Networks (ANN), were employed to establish quantitative relationships between the measured resistivity values and the hydrogeological parameters of interest (Fig. 4).

These parameters include aquifer thickness, porosity, permeability, and hydraulic conductivity. Model training and validation were carried out using available borehole constrained lithologs, and some laboratory estimated data, which worked together to ensure robust calibration and minimize generalization of errors.

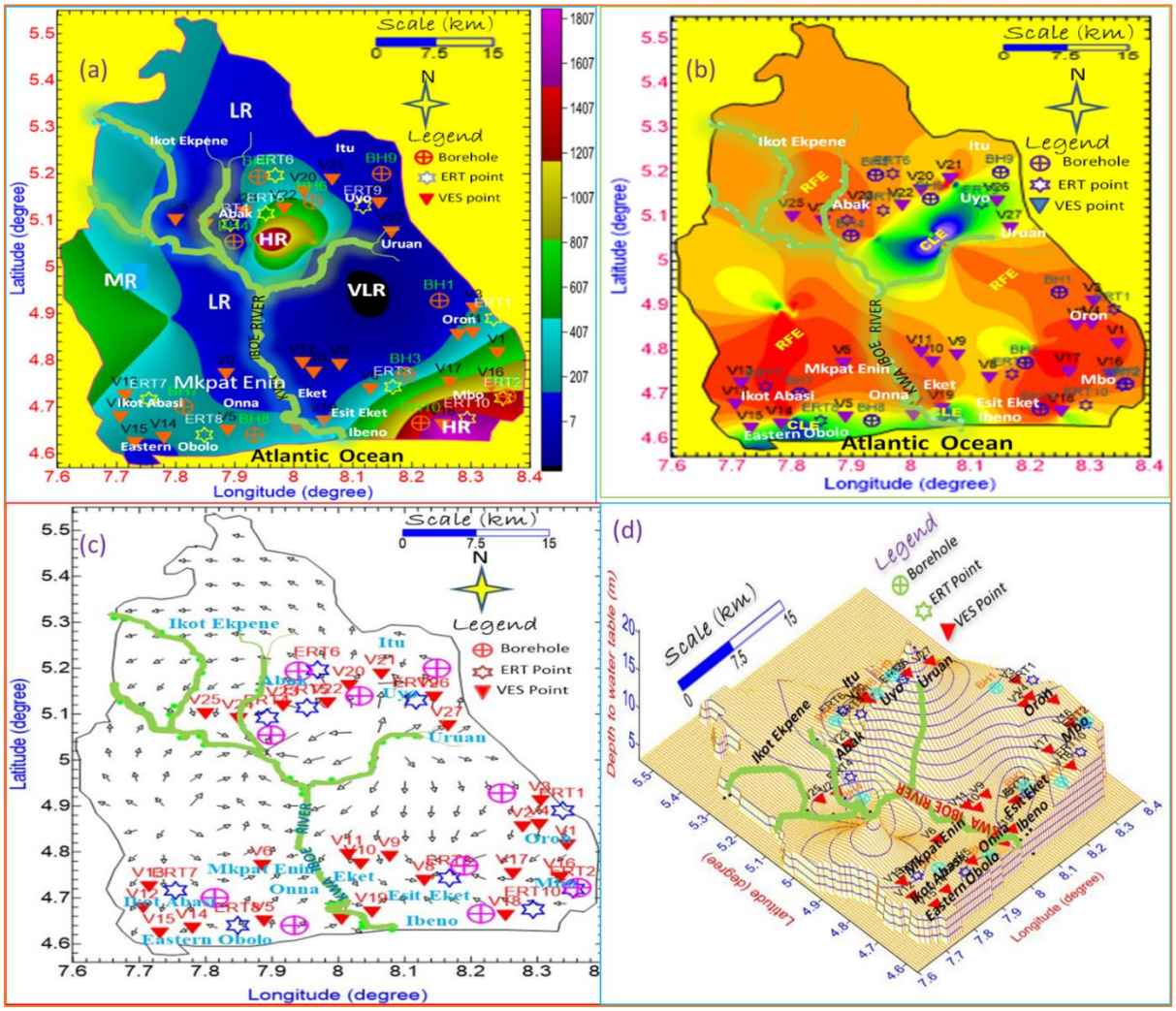

Fig. 7: Diagram illustrating the resistivity distribution of the water-bearing units, along with maps derived from the digital elevation model (DEM) and water table data in the KIRC. (a) Aquifer system resistivity map, characterized by high resistivity (HR), moderate resistivity (MR), low resistivity (LR), and very low resistivity (VLR); (b) relief-shaded map from the DEM showing relatively flat elevation (RFE) and critically low elevation (CLE); (c) grid vector map showing regular and diffuse patterns of flow directions; and (d) 3-D wireframe map showing variations in elevation. The river channel aquifers are categorized based on resistivity as follows: a small portion with very low resistivity (VLR), moderate resistivity (MR), and high resistivity (HR).

To assess the predictive performance of the models, standard diagnostic metrics such as the coefficient of determination (R^2), root mean square error (RMSE), and feature importance rankings were utilized. (Driba *et al*., 2024). This facilitated the identification of critical input features and improved model interpretability. After validation, the trained models were used to generate predictive estimates of the hydrogeological variables, which were then spatially interpolated using geostatistical methods and mapped via GIS platforms.

The final outputs included both two-dimensional (2D) cross-sectional maps and three-dimensional (3D) block models that depict the spatial distribution of aquifer properties across the study area. These visualizations reveal the

lateral and vertical heterogeneity of the subsurface, thereby delineating zones of high groundwater potential and supporting the identification of optimal sites for further hydrogeological investigation.

In essence, this integrated predictive modelling framework offers a cost-effective and scientifically rigorous alternative to conventional invasive methods (Driba *et al.*, 2024). By leveraging the synergistic capabilities of geoelectrical surveying and data-driven modelling, it enhances aquifer characterization and facilitates sustainable groundwater resource management, particularly in hydrologically complex, river-influenced terrains.

4.0 Discussion of results

This study deploys both primary and secondary geoelectric indices to predictively model aquifer properties by examining the influence of the shallow subsurface (layers 1 and 2) on the deeper aquifers (layers 3 and 4) within the Kwa Iboe River channel. A total of 27 Vertical Electrical Sounding (VES) curves and complementary Electrical Resistivity Tomography (ERT) tomograms were analyzed to derive key geoelectric parameters, including bulk water resistivity (BWR), porewater resistivity (PWR), porosity, aquifer thickness, depth to aquifer, formation factor, tortuosity, hydraulic conductivity, permeability, and transmissivity. Topography and sediment distribution significantly influence aquifer behavior (Ekanem *et al*., 2025). Hydraulic conductivity also varies: flatter, loosely packed regions support greater flow, while steeper, compact zones impede movement. High-yield zones (e.g., VES 10, 12, 13, 18) demonstrate favorable aquifer characteristics conducive to sustainable groundwater exploitation, supporting borehole drilling, solar-powered pumping, and piped systems in rural and peri-urban areas, in line with Sustainable Development Goal 6. Conversely, low-yield zones (e.g., VES 1, 7, 14, 20) are marked by shallow or discontinuous aquifers with limited capacity and heightened contamination risks, often associated with low BWR values (<20 Ωm), salinity, waste infiltration, or proximity to rivers.

By integrating VES, ERT, and hydrogeological parameters, the study establishes robust data-driven relationships for evaluating aquifer hydraulics and assessing the influence of shallow layers on deeper ones within the Kwa Iboe River Channel (KIRC). The resistivity data, systematically acquired and cross-validated with borehole lithological records, produce a detailed spatial representation of subsurface conditions. As demonstrated in Figure 3 and Table 1, vertical resistivity sections from VES sites correspond well with lateral ERT profiles, revealing high-resolution images of lithological variability and aquifer structure (Ekanem *et al*., 2025; George *et al*., 2011a).

A key observation is the resistivity inversion in Layer 2, primarily driven by regional hydrodynamic factors such as recharge intensity, saturation variability, and proximity to the river. In the coastal and lowland towns of Oron, Eket, and Ikot Abasi, saltwater intrusion, aggravated by tidal fluctuations, seasonal rainfall, over-abstraction, and land reclamation, lowers resistivity and aquifer thickness, signaling rising freshwater vulnerability due to seawater infiltration and sediment compaction (George & Thomas, 2024).

Depth analyses further confirm vertical heterogeneity within the subsurface. Layer 1 ranges from 0.6 to 14.1 meters (avg. 2.7 m), Layer 2 spans 2.7 to 104.3 meters (avg. 36.6 m), and Layer 3 extends from 36.8 to 95.7 meters (avg. 63.4 m) (see Table 2). These variations reflect the stratigraphic complexity of the Benin Formation in the Niger Delta, shaped by facies transitions and localized tectonic influences that disrupt hydraulic continuity (George *et al.*, 2016; Ikpe *et al*., 2022).

Resistivity values vary widely, often with coefficients of variation exceeding 100%,

highlighting significant hydrological and geotechnical heterogeneity (Zamanian *et al.*, 2024). These variations are influenced by seasonal recharge, sediment textures, and tidal action (Werner *et al*., 2013; Ekanem *et al*., 2025). Regionally, the southern coastal belt shows higher resistivity in the surface layer, suggesting drier or more consolidated materials, while Layer 2 exhibits alternating zones of low and high resistivity, indicative of variable saturation and lithological transitions. In deeper zones, especially Layer 4, anisotropic resistivity trends indicate complex recharge–discharge dynamics controlled by topography, lithofacies, and anthropogenic pressures (George *et al*., 2011 b).

Enhanced saturation and conductivity in Layers 2 and 3, especially within unconfined aquifer zones, are evidenced by resistivity values ranging from 35.4 to 104.3 Ωm, with an average of 550.7 Ωm. These zones support moderate to high groundwater yields. However, saltwater intrusion remains a concern in coastal areas, where increased salinity lowers resistivity and reduces effective aquifer thickness. When compounded by excessive pumping and erosion, this leads to groundwater degradation (Sherif & Singh, (1999).

The formation factor (F), relating rock matrix resistivity to porewater resistivity, ranges from 1.4 to 17.5 (avg. 11.5; CV = 42%), with higher values linked to compacted or poorly connected pore systems. Porosity ranges from 0.104 to 0.54 (avg. 0.164; CV = 59%), reflecting the heterogeneous nature of groundwater storage across varying lithofacies. Zones with high porosity are often more productive but may also be more prone to contamination.

Tortuosity, which describes flow path complexity, varies from 0.9 to 1.3 (avg. 1.2; CV = 10%). Lower tortuosity indicates more direct flow paths, typically found in high-permeability zones but also correlates with greater vulnerability to surface-sourced contamination, especially in shallow, unconfined aquifers near the river. Hydraulic conductivity values span 0.52 to 31.45 m/day (avg. 7.2 m/day; CV = 134%), driven by differences in sediment texture and packing, which affect groundwater flow rates and recharge efficiency. Transmissivity ranges from 18.72 to 1988.27 m²/day (avg. 411.1 m²/day), integrating conductivity and aquifer thickness. Based on Okogbue and Omonona's (2013) classifications in Table 3: Intermediate transmissivity zones (10–100 m²/day) are suitable for small-scale supply, high transmissivity (100–1000 m²/day) supports municipal or community use, and very high transmissivity (>1000 m²/day) is fit for large-scale development. These classifications help guide sustainable groundwater extraction, prioritize protection, and inform regulation efforts.

In general, the hydrogeophysical model developed in this study captures the complex interplay of lithology, resistivity, aquifer dynamics, and river-induced recharge processes within a dynamic deltaic environment. The integration of VES, ERT, and borehole data provides a powerful framework for stratigraphic and hydraulic characterization, supporting long-term groundwater management, contamination risk assessment, and resource sustainability in the Kwa Iboe catchment.

4.1 Spatiotemporal spread parameters

The primary and secondary geoelectric indices measured/estimated were mapped in 2D maps to show the visual distribution of aquifer system properties in the study area. The diagram in Fig. 5 illustrates the geo-resistivity distribution across four successive subsurface layers, each revealing crucial insights into the lithological and hydrological configuration influenced by the freshwater dynamics of the Kwa Iboe River channels. In Layer 1 (Fig. 5a), the shallow subsurface displays patches of low resistivity (LR) zones near the riverbanks, indicative of saturated silty or clayey sediments with high moisture content. Moderate resistivity (MR)

regions suggest a transitional sediment mix with possible fine sand and moderate saturation. The high resistivity (HR) zones occur farther from the river, likely representing unsaturated, coarse-grained, or consolidated lithologies. As depth increases to Layer 2 (Fig. 5b), LR zones remain predominant in channel-adjacent regions, confirming persistent saturation due to lateral recharge. However, MR zones expand, reflecting increased heterogeneity and possible infiltration pathways that allow for partial drying or mineralogical transitions (Ekanem *et al*., 2024). In Layer 3 (Fig. 5c) and Layer 4 (Fig. 5d), the deeper formations show a shift with increasing HR dominance in some distal parts, likely reflecting more compacted, zones with minimal groundwater influence. These resistivity patterns collectively illustrate the influence of the Kwa Iboe River in shaping aquifer properties through vertical and lateral recharge, lithofacies variation, and sediment transport dynamics. The 2D map in Fig. 6 focuses on the hydrodynamic behavior of the aquifer systems by spatially distributing four key hydraulic parameters: porosity, hydraulic conductivity, permeability, and transmissivity.

In Fig. 6a (porosity map), zones of high porosity (HP) correlate with areas close to the river channels, suggesting loosely packed alluvial deposits that facilitate high water storage capacity (MacDonald et al., 2012). Moderate (MP) and low porosity (LP) zones delineate transitions into more compact or fine-grained materials such as silt or clay. The porosity trends align spatially with Fig. 5's LR zones, reinforcing the interpretation of saturated, conductive zones. The display in Fig. 6b (hydraulic conductivity) reveals moderate (MHC) to low hydraulic conductivity (LHC) zones, indicating variability in pore connectivity despite high porosity. This suggests that while some zones store water effectively, their ability to transmit it may be limited by pore throat size or sediment compaction. The hydraulic conductivity data complements Fig. 6c (permeability), where relatively low (RLP) and moderately high permeability (MHP) distributions highlight the spatial complexity of fluid movement, especially in river-adjacent aquifers where recharge is intermittent and sediment sorting is uneven. Again, Fig. 6d (transmissivity) maps the vertical integration of these properties. Zones of relatively very high transmissivity (RVHT) appear near the main water channels, confirming enhanced groundwater flow potential due to both higher saturated thickness and favorable grain connectivity (Ekanem *et al*., 2025). Relatively low transmissivity (RLT) areas may indicate deeper, compacted zones or areas of lower saturation. The map in Fig. 7 integrates resistivity, elevation, and water table characteristics to contextualize aquifer behavior within the topographic and hydrologic framework of the KIRC.

The 2D map in Fig. 7a (resistivity of water-bearing units) again delineates very low resistivity (VLR) zones aligned along the river paths, reflecting saturated, conductive materials (e.g., clay-rich or fine sand zones with high water content). Moderate (MR) and high resistivity (HR) zones are more pronounced away from the river, denoting coarser materials. The demonstration in Fig. 7b (DEM relief-shaded map) identifies relatively flat elevation (RFE) zones aligning with VLR areas, confirming topographic lows that serve as natural recharge zones. The critically low elevation (CLE) zones signify potential zones of flooding or ponding, increasing aquifer saturation and reducing resistivity (Ekanem *et al.*, 2025). The map in Fig. 7c (grid vector map) demonstrates flow direction patterns that transition from regular (well-organized) near the channel to more diffuse and chaotic outward. This reflects channel-induced directional flow and basin-wide discharge zones. Also, Fig. 7d (3-D wireframe elevation map) captures subtle elevation differences that influence hydraulic gradients. Aquifer zones with significant relief

variation indicate stronger groundwater flow potential due to gravitational gradients, while flat zones suggest areas of slower recharge or stagnation (Ekanem *et al*., 2025).

4.2 Synthesis of Hydrogeophysical Behavior

Across all three Figs. 5-7, a consistent hydrogeological theme emerges: the Kwa Iboe River channel significantly influences aquifer structure, recharge, and dynamics (George *et al*., 2017). The low resistivity zones and high porosity-transmissivity zones near the river are indicative of productive aquifers, while distal regions display higher resistivity, lower transmissivity, and greater elevation, correlating with more semi-confined conditions (George *et al*., 2023). The integration of geophysical, hydraulic, and topographic data affirms the critical role of river-aquifer interaction in shaping the hydrogeological framework of the KIRC region. The primary and secondary geoelectric indices were used to predictively model the influence of shallow layers (Layer 3 and 4) on the relatively deeper layers (Layer 3 and 4).

4.3 Predictive Modelling

This study adopts an integrated predictive modelling approach to estimate hydrogeoelectrical behavior across subsurface formations, with a focus on aquifers along water channels in Akwa Ibom State, Southern Nigeria. By establishing mathematical and machine learning-based relationships between surface-measured resistivity values and deeper subsurface properties, the model aims to reduce reliance on invasive, costly drilling methods for aquifer characterization (Alam *et al*., 2025).

As illustrated in Fig. 4, apparent resistivity values derived from Vertical Electrical Sounding (VES) and Electrical Resistivity Tomography (ERT) surveys serve as the primary input data. The resistivity parameters, denoted as ρ_1, ρ_2, ρ_3, and ρ_4, correspond to progressively deeper geoelectric layers, with ρ_1 and ρ_2 representing shallow inputs and ρ_3 and ρ_4 representing relatively deeper target outputs. Linear regression was initially employed to establish empirical relationships that link deeper resistivity layers (ρ_3 and ρ_4), associated with major active aquifers, to shallower layers (ρ_1 and ρ_2). The resulting models are expressed in equations 11 and 12:

$$\rho_3 = 0.037\times\rho_1 + 0.222\times\rho_2 + 524.668 \quad (11)$$

$$\rho_4 = 0.050 \times \rho_1 + 0.256 \times \rho_2 + 604.487 \quad (12)$$

These linear models indicate a positive association between shallow and deeper subsurface resistivity values, with ρ_2 exhibiting a stronger influence than ρ_1. The relatively larger coefficients of ρ_2 suggest that it likely corresponds to a hydraulically active or saturated zone that exerts greater control over the electrical behavior of deeper formations (Driba *et al*., 2024). The intercepts in both models reflect baseline resistivity levels tied to inherent lithological properties and background conductivity. Notably, the modest magnitudes of the regression coefficients point to a mild but consistent sensitivity of deeper resistivity values to variations in upper-layer conditions, a pattern often seen in geo-electrically complex terrains where heterogeneities in stratigraphy, clay content, and moisture distribution affect electrical signal propagation (Ikpe *et al*., 2022).

Recognizing that linear regression may overlook non-linear dependencies, machine learning algorithms, specifically Random Forest and neural networks, were introduced to deepen the analysis and improve predictive accuracy (Fig. 4). Feature importance results from the Random Forest model (Fig. 8) reveal how ρ_1 and ρ_2 contribute to predicting ρ_3 and ρ_4. In Fig. 8(b), which targets ρ_3, the importance values are nearly balanced: ρ_1 contributes 50.7%, while ρ_2 contributes 49.3%. For ρ_4, as shown in Fig. 8(a), the contributions slightly reverse, ρ_1 at 49.8% and ρ_2 at 50.2%. These marginal differences imply that both variables play complementary and nearly equivalent roles in influencing the

model's outputs. Unlike the linear model, Random Forest captures more flexible relationships by accounting for variable interactions and non-linearities without assuming a predefined functional form.

To further investigate potential non-linear interactions that even ensemble tree-based methods might partially obscure, neural network models were applied. These models assigned feature importance scores of 42% and 58% to ρ_1 and ρ_2, respectively, in the prediction of ρ_3, and 41% and 59%, respectively, for predicting ρ_4. The consistently higher importance assigned to ρ_2 aligns with findings from both linear and Random Forest models but with slightly sharper contrast, highlighting the neural network's sensitivity to subtle non-linear interaction

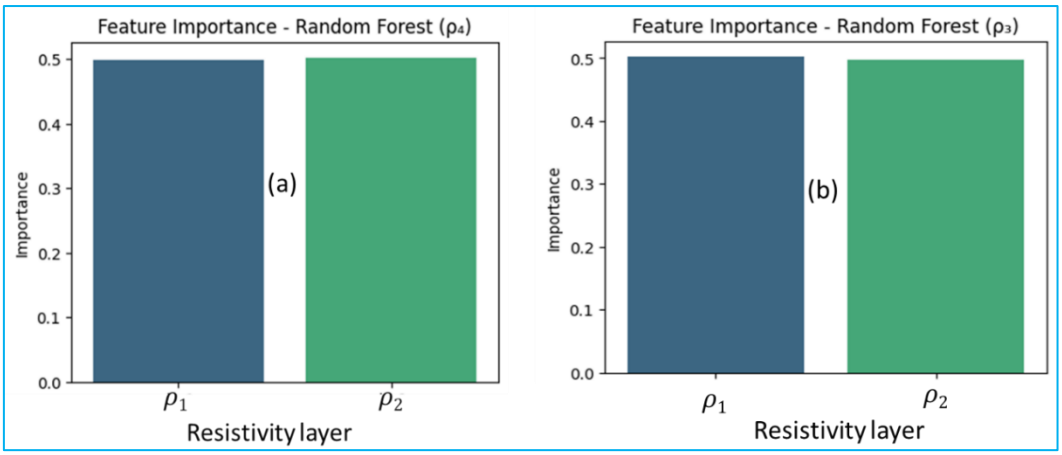

Fig. 8: Relative importance from (a) random forest (ρ_4) and (b) random forest (ρ_3)

Together, these modeling approaches paint a coherent and nuanced picture. Linear regression provides a foundational understanding of the relationships, revealing general trends and sensitivities. Random Forest extends this by uncovering interaction effects and enabling flexible, non-linear mappings. Neural networks further enhance interpretability by resolving finer-scale dependencies that may be masked in other models. Across all frameworks, the repeated emergence of ρ_2 as a slightly more influential predictor underscores its critical role in subsurface resistivity dynamics, while the balanced contributions of both ρ_1 and ρ_2 reflect their combined utility in reliably estimating deeper aquifer characteristics.

The plot in Fig. 9 presents a comparative analysis of predicted versus actual resistivity values for two target layers (ρ_3 and ρ_4) using three different modelling approaches: Neural Network, Random Forest, and Linear Regression. Each sub-plot includes a red dashed reference line representing ideal predictions (i.e., predicted = actual), with the degree of scatter from this line indicating model accuracy. The models were evaluated based on both visual alignment of prediction points and statistical performance metrics such as Root Mean Square Error (RMSE) and Coefficient of Determination (R^2).

In Fig. 9a, the neural network model applied to ρ_3 prediction shows a moderate spread of predicted values around the ideal line. Although some clustering is observed near the center, the scatter becomes more pronounced for higher resistivity values, suggesting inconsistent generalization across the range. The RMSE for this model is relatively high, while the R^2 value indicates a moderate level of explained variance. This reflects the neural network's limited ability to fully capture the complex resistivity-depth relationship at this layer, possibly due to data nonlinearity or model overfitting in mid-range resistivity zones.

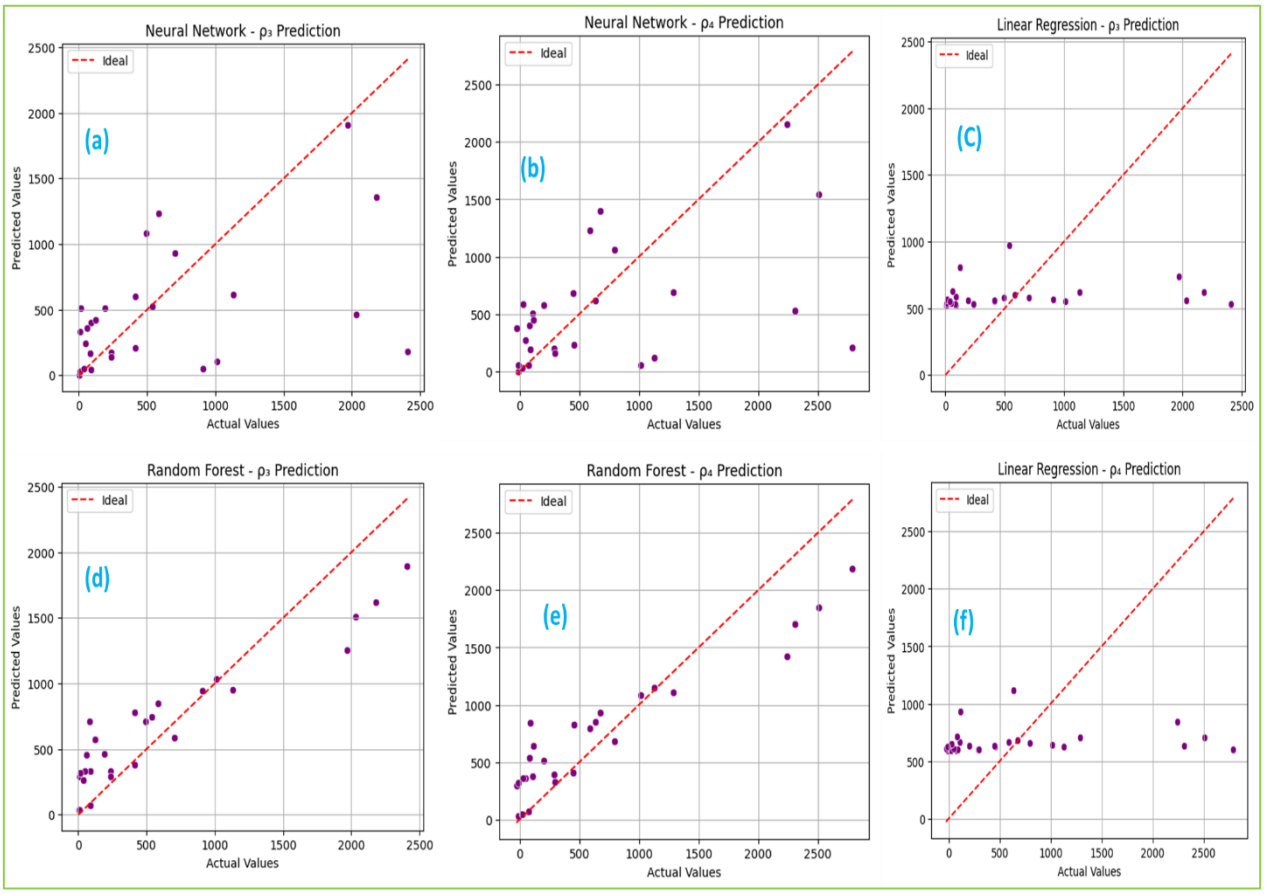

Fig. 9: Predictive Performance Evaluation of Neural Network, Random Forest, and Linear Regression Models for Subsurface Resistivity Estimation

In contrast, Fig. 9b shows the neural network's performance in predicting ρ_4. Here, a modest improvement is evident, with a tighter alignment of predicted values to the ideal line compared to ρ_3. The reduced scatter and more linear trend signify a better learning of resistivity behavior at deeper depths. This improvement is quantitatively supported by a lower RMSE and higher R^2, demonstrating that the neural network adapts more effectively to patterns present in the deeper subsurface layers.

The performance of the linear regression model is illustrated in Fig. 9c and 9f for ρ_3 and ρ_4 predictions, respectively. In both cases, the model exhibits underfitting characteristics, with predictions narrowly distributed and failing to capture the full range of actual resistivity values. This is especially evident in ρ_3 predictions (Fig. 9c), where predicted values do not deviate significantly despite variations in actual values. The low R^2 values and high RMSE reinforce the inadequacy of linear regression for modeling the nonlinear, multilayered structure of the subsurface environment. A similar trend is seen in ρ_4 predictions (Fig. 9f), where the model's performance remains poor, reaffirming its inability to handle nonlinear relationships typical of geoelectrical datasets.

The Random Forest model, as shown in Figs. 9d and 9e, delivers the most promising results. For ρ_3 predictions (Fig. 9d), the scatter plot shows a strong clustering of points along the ideal line, indicating that the model successfully captures the nonlinear patterns governing subsurface resistivity variations. This is further substantiated by the lowest RMSE among all models and a significantly high R^2, suggesting excellent predictive reliability and minimal error. The performance further improves in Fig, 9e, where Random Forest is used to predict ρ_4. The model demonstrates exceptional generalization, with points closely aligning with

the predicted = actual line, reflecting its robustness in learning deeper-layer resistivity structures (Zamanian et al., 2024). The nearly perfect R^2 score and minimal RMSE affirm Random Forest's superiority in handling both shallow and deeper resistivity predictions.

In general, the comparative results indicate that Random Forest outperforms both Neural Network and Linear Regression models in predicting subsurface resistivity. The neural network offers moderate performance, with better results for deeper layers (ρ_4), while linear regression consistently underperforms due to its inability to capture the complex, nonlinear nature of subsurface geoelectrical distributions. These findings validate the utility of ensemble tree-based models in geophysical modelling applications, particularly for data-driven predictions of hydrogeological parameters.

The set of plots presented in Fig. 10 panels (a–f) provides a comparative evaluation of three supervised machine learning models, Random Forest, Ridge Regression, and Neural Network, in their capacity to predict subsurface layer thicknesses, specifically Layer 3 (h_3) and Depth 3 (d_3). These predictions are assessed using scatter plots of actual versus predicted values, with Mean Squared Error (MSE) and the coefficient of determination (R^2) serving as the primary metrics for quantifying model performance. These metrics are fundamental in determining not only how closely the predictions align with observed values but also how well the models explain the variability in the dataset (Zamanian et al., 2024).

In predicting Layer 3 thickness, the Random Forest model, as shown in Fig. 10 panel (a), displays a relatively high MSE of 145.74 and a low R^2 of 0.13, signaling weak predictive accuracy. The dispersion of points away from the red identity line suggests the model struggles to learn the underlying structure of the data, which could be a consequence of overfitting to noise or underfitting due to insufficient model complexity. These limitations are likely aggravated by a small sample size, which hinders the ensemble method's typical ability to generalize.

Ridge Regression, illustrated in Fig. 10 panel (b), outperforms the Random Forest model, achieving a lower MSE of 72.63 and a higher R^2 of 0.57. The predicted values cluster more tightly around the identity line, indicating a more reliable approximation of the actual values. The improved performance is likely due to the influence of L2 regularization, which effectively controls for overfitting by penalizing large coefficients. This is particularly beneficial in small or collinear datasets, as it stabilizes the model and enhances generalization.

On the other hand, the Neural Network model in Fig. 10 panel (c) exhibits the weakest performance for h_3 prediction, with the highest MSE of 216.18 and a negative R^2 value of -0.29. A negative R^2 implies that the model performs worse than a simple mean-based prediction. The wide deviation of predicted values from the identity line reveals a failure to learn the data distribution, which could stem from excessive model complexity, inadequate regularization, or insufficient training data. Neural networks are known to require substantial datasets and careful tuning to perform effectively, especially in domains with complex but sparse data like geotechnical measurements.

A similar trend is observed when these models are applied to the prediction of d_3 thickness, as shown in Fig. 10 panels (d–f). The Random Forest model, in Fig. 10 panel (d), slightly improves in predictive power with an R^2 of 0.36 and an MSE of 183.21. However, the improvement is marginal, and the model continues to show limitations in accurately capturing higher actual values, likely due to the same issues of data sparsity and depth-dependent nonlinearity that affected its performance with h_3.

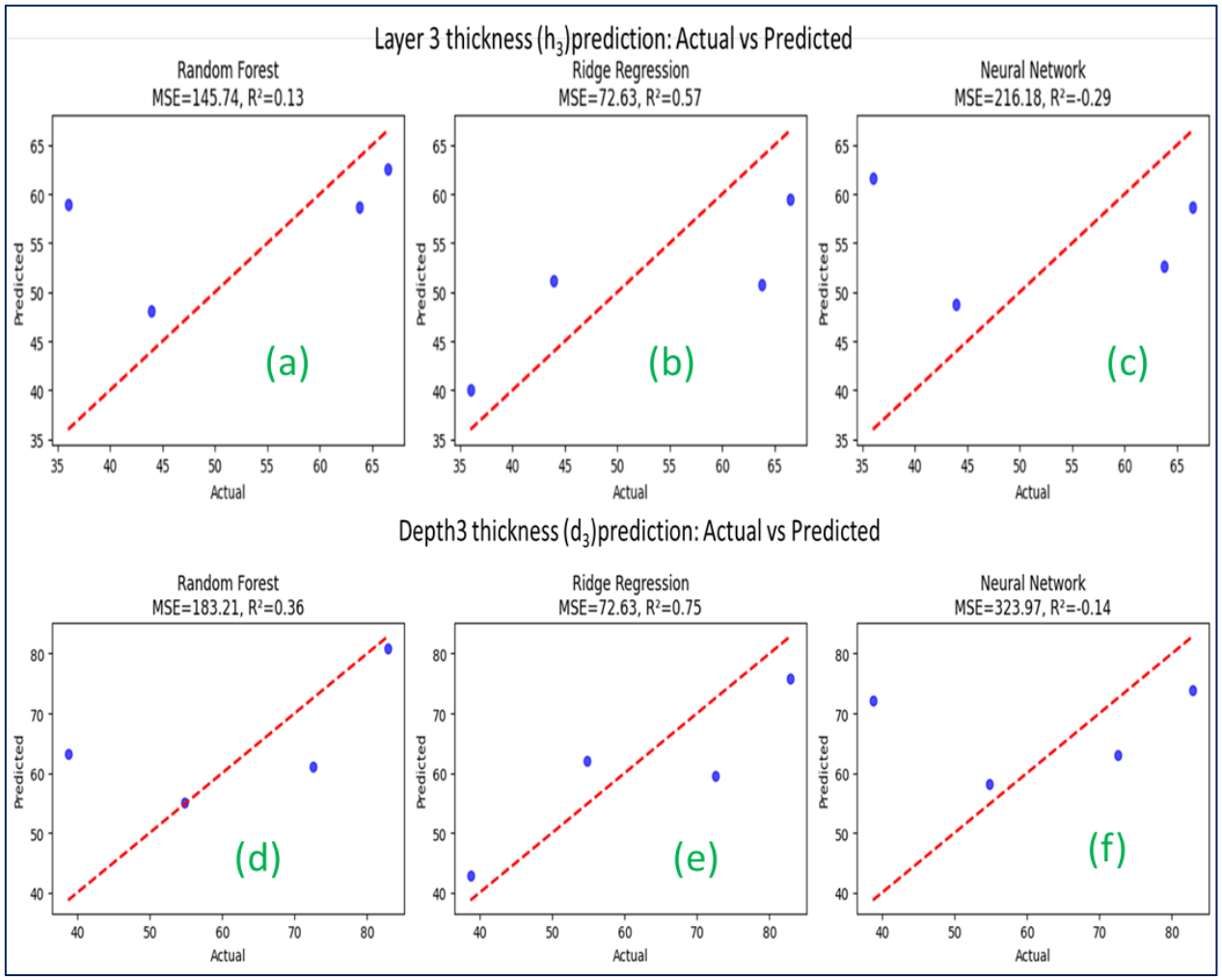

Fig. 10: Comparative Evaluation of Machine Learning Models for Subsurface Layer Thickness Prediction: A Case Study of h_3 and d_3 Layers

Ridge Regression remains the best-performing model for d_3 as seen in Fig 10 panel (e), maintaining an MSE of 72.63 while increasing the R^2 to 0.75. The strong linear relationship between actual and predicted values reflects the model's robustness in capturing the underlying data structure. The consistent performance across both h_3 and d_3 predictions highlights Ridge Regression's suitability for modeling subsurface features, particularly in scenarios constrained by limited or noisy input data.

Conversely, the Neural Network again yields the poorest performance for d_3 prediction, with an MSE of 323.97 and an R^2 of -0.14, as presented in Fig. 10 panel (f). The lack of alignment between predicted and actual values underscores the model's inability to generalize from the training data. This further suggests that neural networks may not be ideal for small datasets without extensive architecture optimization, regularization, and potentially domain-specific feature engineering.

Generally, Ridge Regression emerges as the most reliable and effective model among those evaluated, consistently delivering lower prediction errors and stronger explanatory power for both h_3 and d_3 thicknesses. The Random Forest model shows modest utility, capturing general trends but failing to offer precise or consistent predictions. Neural Networks perform the worst in both cases, likely due to their data-hungry nature and sensitivity to overfitting in low-sample environments (Chala & Ray, 2023). This study underscores the critical role of model selection, regularization strategies, and data volume in developing accurate

predictive tools for geotechnical and subsurface modeling applications.

The integration of statistical correlation analyses further strengthened the modelling framework. A Pearson binary correlation coefficient matrix quantified the degree of linear relationships between geophysical and hydrogeological variables (Fig.11). Notably, bulk resistivity (ρb) and water resistivity (ρw) showed a very strong positive correlation (r = 0.99), confirming the influence of fluid conductivity on subsurface resistivity, a key factor in assessing salinity and aquifer water quality. Porosity (Φ) was strongly negatively correlated with hydraulic conductivity (K, r = -0.94) and formation factor (F, r = -0.84), supporting known petrophysical principles such as Archie's Law.

	ρb (Ωm)	h (m)	d (m)	ρw (Ωm)	Φ	F	K (m/day)	K (m/s)	Kp (mD)	T (m^2/day)
ρ_b (Ωm)	1.00									
h (m)	-0.06	1.00								
d (m)	-0.03	0.86	1.00							
ρ_w (Ωm)	0.99	-0.05	-0.01	1.00						
Φ	-0.35	0.13	0.06	-0.29	1.00					
F	0.38	-0.08	-0.03	0.29	-0.84	1.00				
K (m/day)	0.43	-0.07	-0.03	0.36	-0.94	0.91	1.00			
K (m/s)	-0.53	-0.02	-0.10	-0.62	0.04	0.30	0.00	1.00		
Kp (mD)	-0.53	-0.02	-0.10	-0.62	0.04	0.30	0.00	1.00	1.00	
T(m^2/day)	-0.53	-0.02	-0.10	-0.62	0.04	0.30	0.00	1.00	1.00	1.00

Fig. 11: Diagram showing strong positive (coefficients ranging from 0.86 to 1.00: Gold colour) and strong negative (coefficients ranging from -0.94 to -0.84: Blue colour) binary correlations between the measured and estimated aquifer parameters

High positive correlations were also observed between formation factor and hydraulic conductivity (r = 0.91), and nearly perfect correlations between *K*, permeability (K_p), and transmissivity (T), illustrating their mutual dependence in describing aquifer flow behavior. To evaluate the statistical significance of the observed relationships, a p-value matrix and statistically significant correlations shown in Table 4 and Fig. 12, respectively were applied. Among the tested correlations, the relationship between bulk resistivity and water resistivity (ρ_b–ρ_w) yielded a p-value of 0.00, indicating strong statistical significance (true) and confirming its suitability for inclusion in predictive models (Moghadas & Badorreck, 2019). In contrast, correlations such as thickness–transmissivity (*h–T*, p = 0.91) and depth–hydraulic conductivity (*d–K*, *p* = 0.89) exhibited high p-values, suggesting that these relationships are false or not statistically significant and may be due to chance. The diagram in Fig. 12 presents a Boolean heatmap identifying statistically significant correlations ($p < 0.05$) among the measured and derived hydrogeophysical parameters. It underscores the strength of relationships that are not just numerically correlated but also statistically valid. As such, caution is advised when interpreting or including them in model training.

Table 4: P-Value matrix for testing of statistical significance of measured and estimated aquifer parameters

	ρb (Ωm)	h (m)	d (m)	ρw (Ωm)	Φ	F	K (m/day)	K (m/s)	Kp (mD)	T (m^2/day)
ρb (Ωm)	1.00	0.78	0.90	0.00	0.08	0.05	0.03	0.00	0.00	0.00
h (m)	0.78	1.00	0.00	0.82	0.52	0.71	0.72	0.92	0.92	0.91
d (m)	0.90	0.00	1.00	0.95	0.76	0.86	0.89	0.63	0.63	0.63
Pw (Ωm)	0.00	0.82	0.95	1.00	0.15	0.15	0.06	0.00	0.00	0.00
Φ	0.08	0.52	0.76	0.15	1.00	0.00	0.00	0.83	0.83	0.83
F	0.05	0.71	0.86	0.15	0.00	1.00	0.00	0.13	0.13	0.13
K (m/day)	0.03	0.72	0.89	0.06	0.00	0.00	1.00	0.99	0.99	0.99
K (m/s)	0.00	0.92	0.63	0.00	0.83	0.13	0.99	1.00	0.00	0.00
Kp (mD)	0.00	0.92	0.63	0.00	0.83	0.13	0.99	0.00	1.00	0.00
T(m^2/day)	0.00	0.91	0.63	0.00	0.83	0.13	0.99	0.00	0.00	1.00

Interestingly, certain relationships like porosity-hydraulic conductivity (*Φ–K*) and formation factor–hydraulic conductivity (*F–K*) showed numerically strong correlations but failed to meet statistical significance thresholds. This discrepancy is likely attributable to limited sample size or non-linear interactions between variables, which may obscure underlying patterns detectable only with larger datasets or more advanced modeling techniques. This combined statistical framework, leveraging both correlation strength and p-value evaluation, facilitates the selection of robust predictor variables for machine learning applications (Kundu *et al.*, 2024). Parameters such as ρ_b–ρ_w and *Φ*–K_p, which display both high correlation and statistical relevance, serve as reliable inputs for training models like Random Forest, Ridge Regression, and Neural Networks. These models enable accurate estimation of critical hydrogeological parameters while preserving physical interpretability.

Lastly, Fig. 13 presents the Pearson correlation matrix, illustrating both the strength and direction of relationships among hydrogeophysical parameters, with values ranging from -1 to +1. The heatmap reveals strong positive correlations among K, Kp, and T, confirming consistency across different measures of hydraulic conductivity and transmissivity, which enhances their reliability as predictive variables in groundwater modelling. It also highlights strong negative correlations between porosity (Φ) and both formation factor (F) and K, indicating that more porous zones are generally more conductive, characteristic of water-bearing formations. Additionally, bulk density (ρ_b) exhibits notable positive correlations with K and F, suggesting that denser subsurface layers may exhibit increased transmissivity under certain conditions (George *et al.*, 2018).

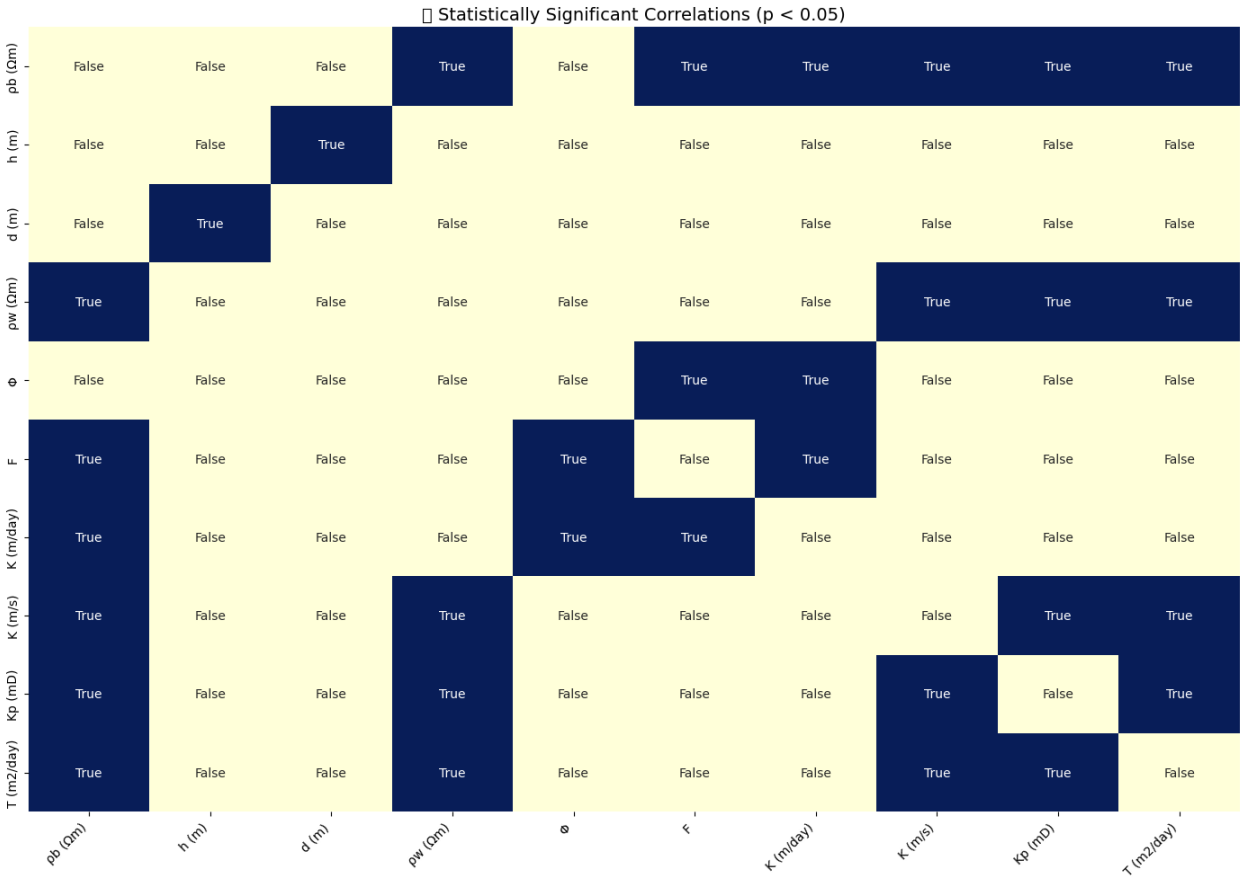

Fig. 12: Statistically Significant Correlations ($p < 0.05$) Among Hydrogeophysical Parameters Derived from Integrated VES Data

In all, the matrix supports the empirical linkage between geophysical indicators and hydrogeological properties, reinforcing their integration in predictive subsurface modelling.

Practically, the modeling approach developed in this study demonstrates that deeper-layer resistivities (ρ_3 and ρ_4), along with key aquifer parameters such as thickness, depth, and hydraulic conductivity, can be effectively inferred from shallow-layer resistivity data. The improved accuracy and adaptability of machine learning, particularly ensemble-based and regularized models, support robust predictive capabilities even in complex geological settings or areas with sparse data.

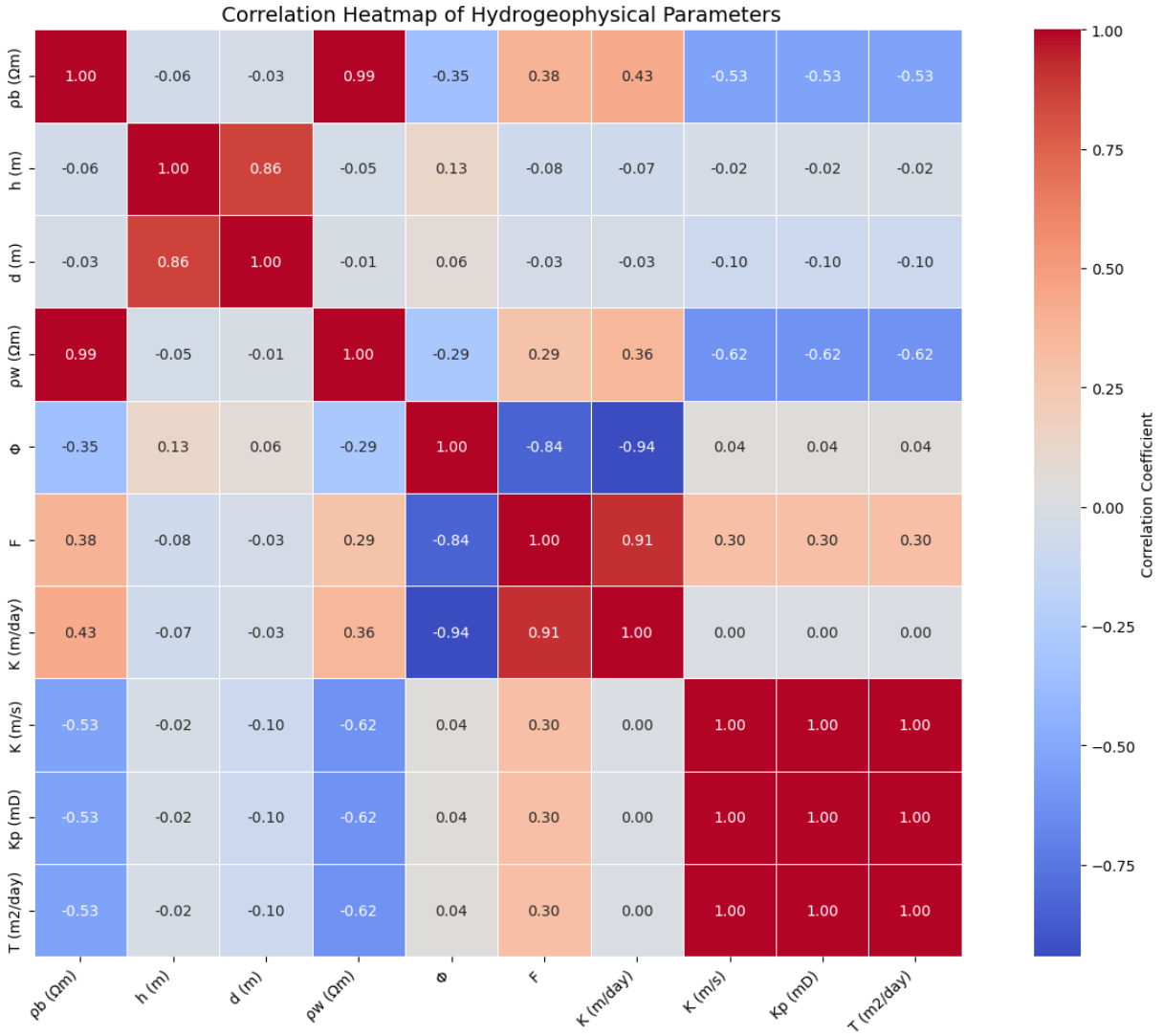

Fig. 13: Pearson Correlation Heatmap of Hydrogeophysical Parameters Along the Water Channel in Akwa Ibom State.

5.0 Concluding remarks

This study demonstrates the practical value of an integrated hydrogeophysical modelling approach for groundwater assessment in river-influenced terrains of Southern Nigeria. By combining Vertical Electrical Sounding (VES), Electrical Resistivity Tomography (ERT), and machine learning, the framework effectively predicts key aquifer properties such as porosity, transmissivity, and hydraulic conductivity, supporting informed water resource planning.

Among the models tested, Random Forests showed superior performance in predicting subsurface resistivity values, while Ridge regression effectively estimated aquifer depth and thickness. The strong correlations observed between geoelectrical and hydrogeological parameters validate the model's reliability and highlight the interconnectedness of subsurface electrical and hydraulic behavior.

Hydrogeological analysis confirmed high-yield aquifers with strong transmissivity and hydraulic conductivity, guiding efficient borehole placement, with transmissivity and hydraulic conductivity values indicative of favorable groundwater flow conditions. These findings reinforce the role of resistivity-based, non-invasive methods in identifying high-yield aquifer zones and optimizing borehole placement.

In general, the proposed methodology reduces exploration costs, limits reliance on invasive drilling, and offers a scalable solution for

groundwater development in sedimentary environments across tropical regions.

Funding: The project was funded by the authors

Declaration of Competing Interest: The authors declare that they have no known competing financial interests or personal relationships that could have appeared to influence the work reported in this paper.

Acknowledgements: The authors would like to express their gratitude to their colleagues in the Geophysics Research Group (GRG) at Akwa Ibom State University for their support during field data collection and for their contributions to the manuscript editing process.

References

Adelana, E. M. & Taylor, R. G. (2008) *Groundwater Resources in Nigeria: A Review of Occurrence and Quality* (CRC Press, New York, 2008).

Akpan, A. E., Ekwok, S. E., Ben, U. C., Ebong, E. D., Thomas, J. E., Ekanem, A. M., George, N. J., Abdelrahman, K., Fnais, M. S., Eldosouky, A. M., Andráš, P., & Alarifi, S. S. (2023). Direct Detection of Groundwater Accumulation Zones in Saprock Aquifers in Tectono-Thermal Environments. *Water*, 15(22), 3946. https://doi.org/10.3390/w15223946

Alam, M. J. B., Gunda, A., & Ahmed, A. (2025). Machine Learning Approach to Model Soil Resistivity Using Field Instrumentation Data. Geotechnics, 5(1), 5. https://doi.org-/10.3390/geotechnics5010005

Anomohanran, I. O. (2011). Geophysical investigation of groundwater potential in Ukelegbe, Nigeria, using vertical electrical sounding method, J. *Appl. Sci. Environ. Manag.* **15**, 241–246.

Archie, G. E. (1942). The Electrical Resistivity Log as an Aid in Determining Some Reservoir Characteristics. Transactions of the AIME, 146, 54-62.

Asfahani, J., Aretouyap, Z. & George, N. (2023). Hydraulic characterization of the Adamawa-Cameroon aquifer using inverse slope method, *Water Practice and Technology* 18 (3), 547-562

Carman, P. C., (1937). Fluid flow through granular beds. Trans. Inst. Chem. Eng. 15, 150–166.

Carman, P.C., (1956). Flow of Gases through Porous Media

Chala, A. T. & Ray, R. (2023). Assessing the Performance of Machine Learning Algorithms for Soil Classification Using Cone Penetration Test Data. *Appl. Sci.*, *13*, 5758.

Driba, D. L., Emmanuel, E. D. & Doro, K. O. (2024). Predicting Wetland Soil Properties Using Machine Learning, Geophysics, and Soil Measurement Data. *J. Soils Sediments*, *24*, 2398 – 2415.

Ekanem A. M., George, N. J. & Thomas, J. E. (2024). Investigation of aquifer storage properties and groundwater contamination risk potential using an electrical resistivity technique: a sedimentary environment case study, *Water Practice and Technology*, 19 (8): 3350–3372, https://doi.org/10.2166-/wpt.2024.203

Ekanem A. M., Ikpe E. O., George N. J. & Thomas J. E. (2022a). Integrating geoelectrical and geological techniques in GIS-based DRASTIC model of groundwater vulnerability potential in the raffia city of Ikot Ekpene and its environs, southern Nigeria. *Int. J. Energy Water Res*. https:// doi. org/ 10. 1007/ s42108- 022-00202-3

Ekanem K. R., George N. J. & Ekanem A. M. (2022b). Parametric characterization, protectivity and potentiality of shallow hydrogeological units of a medium-sized

housing estate, Shelter Afrique, Akwa Ibom State, Southern Nigeria. *Acta Geophysica* 70 (2): 879 – 895

Ekanem, K. R., George, N. J., Ekanem, A. M., Udosen, N. I. & Thomas, J. E. (2025). Georesistivity assessment of lithological and hydrodynamic factors in groundwater sanitation of Akwa Ibom river channel aquifer system, *Geosystems and Geoenvironment*, 4(3), 100411, https://-doi.org/10.1016/j.geogeo.2025.100411.

Emmanuel C. C. (2013). Monitoring the Quality of Groundwater and Leachate Contamination near Waste Dump in Coastal Plain Sand Aquifer. M.Sc. Thesis, University of Calabar, Calabar.

Etu-Efeotor, J. O. & Akpokodje, E. G. (1990) Aquifer Systems of Niger Delta. JMG Vol. 26 No 2, 279-284.

Freeze, B & Cherry, J. A. (1979) *Groundwater* (Prentice Hall, New Jersey, 1979).

George, N., Obianwu, V., & Udofia, K. (2011a). Estimation of Distribution of Aquifer Hydraulic Parameters in the Southern Part of Akwa Ibom State, Southern Nigeria Using Surficial *Geophysical Measure-ments. International Review of Physics*, 5(2), 53 - 59.

George, N. J., Obianwu, V. I. & Obot, I. B. (2011b). Laboratory estimation of aquifer effective porosities from core samples obtained during borehole drilling in parts of the Niger Delta Region, South-eastern Nigeria, *Adv Appl Sci Res Pelagia Res Libr*., 2(1), 153-162

George N. J., Ibanga, J. I. & Ubom. A. I. (2015a). Geoelectro - hydrogeological indices of evidence of ingress of saline water into freshwater in parts of coastal aquifers of Ikot Abasi, southern Nigeria, *Journal of African Earth Sciences*, Egypt, 109, 37 – 46, http://dx.doi.org/10.1016-/j.jafrearsci.2015.05.001

George N. J., Ibuot J., C. & Obiora D. N. (2015b): Geoelectrohydraulic parameters of shallow sandy aquifer in Itu, Akwa Ibom State (Nigeria) using geoelectric and hydrogeological measurements, *Journal of African Earth Sciences*, 110, 52-63, http://dx.doi.org/10.1016/j.jafrearsci.2015.06.006.

George N. J., Agbasi O. E., Umoh J. A., Ekanem A. M., Ejepu J. S., Thomas J. E. & Udoinyang I. E. (2022b). Contribution of electrical prospecting and spatiotemporal variations to groundwater potential in coastal hydro-sand beds: a case study of Akwa Ibom State, Southern Nigeria. *Acta Geophys*. 71, 2339–2357. https://doi.org-/10.1007/s11600-022-00994-2.

George N. J., Akpan A. E. & Ekanem A. M. (2016). Assessment of textural variational pattern and electrical conduction of economic and accessible quaternary hydrolithofacies via geoelectric and laboratory methods in SE Nigeria: a case study of select locations in Akwa Ibom State. *J Geol Soc India* 88:517–528

George, N. J. & Thomas J. E. (2024). Typification of coastal depositional lithofacies with isophysical and isochemical hydro-sand beds via stratigraphic modified Lorenz plots (SMLP): geohydrodynamical implications and valorization of hydrogeological units, *Acta Geophysica* 72 (2), 1275-1291, https://doi.org/10.1007/-s11600-023-01160-y

George, N.J. (2020). Appraisal of hydraulic flow units and factors of the dynamics and contamination of hydrogeological units in the littoral zones: a case study of Akwa Ibom State University and its Environs, Mkpat Enin LGA, Nigeria. *Natural Resources Research*, 29(6), pp.3771-3788.https://doi.org/10.1007/s11053-020-09673-9.

George, N. J. (2021). Modelling the trends of resistivity gradient in hydrogeological units: a case study of alluvial environment. *Modeling Earth Systems and*

Environment, 7, pp.95 104. https://doi.org-/10.1007/s40808-020-01021-3

George, N. J., Agbasi, O. E., Umoh, A. J., Ekanem, A. M., Udosen, N.I., Thomas , J. E., Aka, M. U. & Ejepu , J. S. (2025) Enhanced contamination risk assessment for aquifer management using the geo-resistivity and DRASTIC model in alluvial settings, *Cleaner Water*, Vol. 3, 100060, https://doi.org/10.1016/j.clwat.2024.10006

George, N. J., Ekanem, A. M., Ibanga, J. I. & Udosen, N. I. (2017). Hydrodynamic implications of aquifer quality index (AQI) and flow zone indicator (FZI) in groundwater abstraction: a case study of coastal hydro-lithofacies in South-eastern Nigeria. *Journal of Coastal Conservation*, 21, pp.759-776. https://doi.org/10.1007-/s11852-017-0535-3

George, N. J., Ekanem, A. M., Obiora, D. N., Ibuot, J. C. & Akpan, A. S. (2021a). Estimating the energy in current signals during electrical sounding: a novel approach. *Arab J. Geosci* 14, 301. https://doi.org/10.1007/s12517-021-06625-2.

George, N. J., Ekanem, A. M., Thomas, J. E. & Ekong, S. A. (2021b). Mapping depths of groundwater - level architecture: implications on modest groundwater-level declines and failures of boreholes in sedimentary environs. *Acta Geophys.*, 69, 1919-1932, 10.1007/s11600-021-00663-w.

George, N. J., Ekanem, A. M., Thomas, J. E., Udosen, N. I., Ossai, N. M. & Atat, J. G. (2024). Electro-sequence valorization of specific enablers of aquifer vulnerability and contamination: A case of index-based model approach for ascertaining the threats to quality groundwater in sedimentary beds. *HydroResearch*, 7, pp.71 - 85. https://-doi.org/10.1016/j.hydres.2023.11.006

George, N. J., Ekanem, K. R., Ekanem, A. M., Udosen, N. I. & Thomas, J. E. (2022a). Generic comparison of ISM and LSIT interpretation of geo-resistivity technology data, using constraints of ground truths: a tool for efficient explorability of groundwater and related resources. *Acta Geophysica*, 70(3), pp.1223-1239. https://-doi.org/10.1007/s11600-022-00794-8

George, N. J., Ibuot, J. C., Ekanem, A. M. & George, A. M. (2018). Estimating the indices of inter-transmissibility magnitude of active surficial hydrogeologic units in Itu, Akwa Ibom State, Southern Nigeria. *Arabian Journal of Geosciences*, 11, pp.1-16.https://doi.org/10.1007/s12517-018-3475-9

George, N. J. & Thomas, J. E. (2023). Groundwater potential and quality assessments of a coastal environment: a case study of the location of Federal University of Technology Ikot Abasi (FUTIA), Akwa Ibom State, Nigeria. *Journal of Coastal Conservation* 27 (4), https://doi.org/10.1007/s11852-023-00956-w

Ghouili, N., Jarraya-Horriche, F., Hamzaoui-Azaza, F., Zaghrarni, M. F., Ribeiro, F. & Zammouri, M. (2020). Groundwater vulnerability mapping using the Susceptibility Index (SI) method: Case study of Takelsa aquifer, Northeastern Tunisia. *J. Afr. Earth Sci.*, 173, Article 104035, 10.1016/j.jafrearsci.2020.104035.

Ibuot J. C., Okeke F. N., George N. J. & Obiora D. N. (2017). Geophysical and physicochemical characterization of organic waste contamination of hydro lithofacies in the coastal dumpsite of Akwa Ibom State, southern Nigeria, Science & Technology: *Water Supply*, 17 (6): 1626-1637, Doi: 10.2166/ws.2017.066.

Ibuot, J. C., Obiora, D. N. & George, N. J. (2024). Evaluation of geohydraulic response properties of hydrogeological units in Littoral hydro-lithofacies in Uyo, Southern Nigeria, *Appl. Water Sci.*, 14 (2024), p. 9, 10.1007/s13201-023-02057-3.

Ikpe E. O., Ekanem A. M., & George, N. J., (2022). Modelling and assessing the protectivity of hydrogeological units using primary and secondary geoelectric indices: a case study of Ikot Ekpene Urban and its environs, southern Nigeria, *Modeling Earth Systems and Environment*. ***8***, *4373–4387. https://doi.org/10.1007/s40808-022-01366-x*

Ikpe, E. O., Ekanem, A. M., George, N. J. & Thomas, J. E. (2025). Geophysical assessment of aquifer protectivity, groundwater potential and flow dynamics in Northern Akwa Ibom state, Nigeria: Implications for sustainable freshwater management, *Geosystems and Geoenvironment* 4, (3), 100401, https://-doi.org/10.1016/j.geogeo.2025.100401

Inim I. J., Udosen N. I., Tijani M. N., Afia U. E. & George N. J. (2020). Time-lapse electrical resistivity investigation of seawater intrusion in coastal aquifer of Ibeno, Southeastern Nigeria, *Applied Water Science*, Germany, 10, 232 (2020), https://doi.org/10.1007/s13201-020-01316-x

Inyang N., George N., Ehibor, I., Ekot, A. & Udo, I. (2024). Ingress of municipal solid waste into water resources: an environmental assessment and monitoring tool near dumpsites in Akwa Ibom State, Nigeria, *Water Practice and Technology* 19 (8): 3182–3202. https://doi.org/10.2-166/wpt.2024.187

Kozeny, J., (1927). Über kapillare Leitung der Wasser in Boden. Royal Academy of Science, Vienna, Proc. Class I 136, 271–306.

Kundu, S.K., Dey, A.K., Sapkota, S.C., Debnath, P., Saha, P.; Ray, A. & Khandelwal, M. (2024). Advanced predictive modelling of electrical resistivity for geotechnical and geo-environmental applications using machine learning techniques. *J. Appl. Geophys.*, 231, 105557

MacDonald, A. Bonsor, M. H. C., Dochartaigh B. É. Ó., & Taylor, R. G. (2012). Quantitative maps of groundwater resources in Africa," *Environ. Res. Lett.* **7**, 024009.

Moghadas, D. & Badorreck, A. (2019). Machine learning to estimate soil moisture from geophysical measurements of electrical conductivity. *Near Surf. Geophys.*, *17*, 181–195

Onwumechili, A. C. & Okonkwo, C. O. (2013) Hydrogeological implications of resistivity variation in Akwa Ibom State, Nigeria," *J. Geophys. Eng.* **10**, 047003.

Sherif, M. M., & Singh, V. P. (1999). Effect of saltwater intrusion on groundwater resources in coastal aquifers. *Hydrological Sciences Journal*, 44(2), 288-294. https://doi.org/10.1080/02626669909492251

Udosen, N.I., Ekanem, A.M. & George, N. J. (2024a). Modeling of aquifer geo-hydraulic characteristics with geo-electrical methods at a major coastal aquifer system in Uyo, southern Nigeria, *Water Practice & Technology* 19 (2), 611-628

Udosen, N. I., Ekanem, A.M. & George, N.J., Thomas J. E.(2024b) Geo-electrostratigraphic assessment of aquifer potential, protectivity, and pliable level of vulnerability within a coastal milieu, *Water Practice & Technology* 19 (5), doi: 10.2166/wpt.2024.125

Udosen, N. I., Ekanem, A. M. & Thomas, J. E. (2024c). Geo-hydraulic characterization of a coastal aquifer system in South-eastern Nigeria with the inverse slope method. *Researchers Journal of Science and Technology*, 4(1), pp.1-20.

Umoh, J, A., George, N. J., Ekanem, A.M., Thomas, J. E. & Emah, J. B. (2022). Approximate delineation of groundwater yield capacity and vulnerability via secondary geo-electric indices and rock-water interaction hydrodynamic

coefficients in a coastal environment, Researchers Journal of Science and Technology, 2(3), 28-54

Uwa, U. E., Akpabio, G. T. & George, N. J. (2019). Geohydrodynamic parameters and their implications on the coastal conservation: A case study of Abak Local Government Area (LGA), Akwa Ibom State, Southern Nigeria, *Nat Resour Res*., Switzerland, 28(2), 349-367, https://-doi.org/10.1007/s11053-018-9391-6

Werner, A. D., Simmons, C. T., & Heilweil, V. M. (2013). Saltwater intrusion processes, investigation, and management: Recent advances and future directions. *Journal of Hydrology*, 505, 3–18. https://doi.org/-10.1016/j.jhydrol.2013.08.016.

Zamanian, M., Asfaw, N. & Chavda, P., Shahandashti, M. (2024). Deep learning for exploring the relationship between geotechnical properties and electrical resistivities. *Transp. Res. Rec.*, *2678*, 659–672.